BACCHUS

Impact of Biogenic versus Anthropogenic emissions on Clouds and Climate: towards a Holistic Understanding

Collaborative Project

SEVENTH FRAMEWORK PROGRAMME
ENV.2013.6.1-2

Atmospheric processes, eco-systems and climate change

Grant agreement no: 603445

Deliverable number:	**D1.3**
Deliverable name:	Preliminary sets of aerosol and cloud data (integration of on-going observations), and respective documentation of observations
WP number:	1
Delivery date:	Project month 36 (30/11/2016)
Actual date of submission:	28/11/2016
Dissemination level:	PU
Lead beneficiary:	TROPOS
Responsible scientist/administrator:	A. Ansmann, J. Atkinson, M.C. Facchini
Estimated effort (PM):	362.74
Contributor(s):	J. Atkinson (ETHZ), F. Ramelli (ETHZ), B. Sierau (ETHZ), S. Sandrini (CNR-ISAC), S. Decesari (CNR-ISAC), M. Paglione (CNR-ISAC), M.C. Facchini (CNR-ISAC), M. Rinaldi (CNR-ISAC); K. Oikonomou (CYI), M. Pikridas (CYI), J. Stavroullas

Contributor(s): (continued)	(CYI), O. Antoniou (CYI), J. Sciare (CYI), C. Keleshis (CYI); U. Pöschl (MPIC), M. Andreae (MPIC), Y. Cheng (MPIC), H. Su (MPIC), C. Pöhlker (MPIC), A. Huffman (MPIC), W. Zhibin (MPIC), J. Ditas (MPIC), M. Kruger (MPIC); H. Bingemer (UOF) J. Schrod (UOF), M. Simon (UOF), A. Kube (UOF), K. Krüger (UOF), M. Rahman (UOF), J. Drücke (UOF), J. Kossmann (UOF), M. Jesswein (UOF), N. Koch (UOF), C. Hartik (UOF), D. Machill (UOF), S. Hack (UOF), P. Hauff (UOF), A. Haunold (UOF); K. Fossum (NUIG), J. Ovadnevaite (NUIG); J. Preissler (NUIG); J. Bühl (TROPOS); A. Ansmann (TROPOS); U. Baltensperger (PSI), G. Motos (PSI), A. Prevot (PSI), J. Schmale (PSI), M. Gysel (PSI); S. Mazon (UHEL), A. Manninen (UHEL), V.-M. Kerminen (UHEL); N. Kivekäs (FMI), G. de Leeuw (FMI), T. Virtanen (FMI); E. Hashimshoni (HUJI); T. Goren (HUJI); D. Giguzin (HUJI); I. Bib (HUJI); S. Levi (HUJI); B. Fischman (HUJI); A. Zippori (HUJI); M. Crooks (UMAN); A. Tofaris (UMAN); P. Connolly (UMAN); B. Pigov (INRNE); V. Ganchev (INRNE); K. Kolev (INRNE); Z. Nedyalkov (INRNE); A. Welti (TROPOS); P. Herenz (TROPOS); R. Calmer (CNRS); K. Sanchez (CNRS); G. Roberts (CNRS); K. Carslaw (ULEEDS); J. Vergara Temprado (ULEEDS)
Estimated effort contributor(s) (PM):	ETHZ: 19.5 PM, CNR-ISAC: 24 PM, CYI: 30 PM, MPI-C: 14.5 PM, UOF: 57.3 PM, NUIG: 33 PM, TROPOS: 51.5 PM, PSI: 16 PM, UHEL: 19 PM, FMI: 5 PM, HUJI: 47.5 PM, UMAN: 17.5 PM, INRNE: 5.44 PM, CNRS: 20.5 PM, ULEEDS: 2 PM
Internal reviewer:	Ulrike Lohmann, Monika Burkert

Deliverable 1.3:

Preliminary sets of aerosol and cloud data (integration of on-going observations) and respective documentation of observations

Work package 1 (WP1) covers the aerosol and cloud observations performed within the framework of BACCHUS. Focus is placed on the characterization of aerosol particles to serve as cloud condensation nuclei (CCN) and ice nucleating particles (INP) based on past and published in-situ measurements, as well as those from new observations (e.g., BACCHUS, Mace Head 2015, Cyprus 2015 and 2016 campaigns). The goal is to establish a global database or database infrastructure (which does not necessarily contain the data physically) of CCN and INP properties for different natural and anthropogenic aerosol types and mixtures around the world. WP1 also deals with vertically resolved field observations of aerosols and clouds in key climate regions from aerosol/cloud lidars and cloud radars, organized in networks (e.g., ACTRIS, Cloudnet) or arranged in super sites within large field campaigns (e.g., BAECC), and by including aircraft observations (e.g., ACCACIA, ACRIDICON). Satellite remote sensing with very high horizontal resolution (e.g., the Visible Infrared Imager Radiometer Suite (VIIRS), on board NASA's Earth-observing satellite NPP) is used to study aerosol-cloud interactions in key regions of global climate and for global change. In the first step, closure studies, validation efforts, quality assurance work and re-analysis of past observations were performed. Here, we report progress in our studies with the main focus on findings from recent field campaigns performed since May 2015.

WP1 is organized in six tasks (Tasks 1.1-1.6):

Task 1.1: Definition of the natural background aerosol and measurement framework for the IN database

Task 1.2: Compilation of geographic differences in IN/CCN

Task 1.3: Quantification of natural (biological, dust) and anthropogenic contributions to IN

Task 1.4: Quantification of biogenic and anthropogenic contribution to organic aerosol and their ability to act as CCN

Task 1.5: Obtaining the vertical structure of aerosols and clouds

Task 1.6: Establishment of a harmonized dataset of aerosol, CCN/IN and cloud microphysical properties

1. Contribution from task 1.1 "Definition of the natural background aerosol and measurement framework for the IN database" (ETHZ, UOC, CNR-ISAC, NUIG, MPI-C, TROPOS) and task 1.2 "Compilation of geographic differences in IN/CCN" (ETHZ, UHEL, FMI, TROPOS, UMAN, CYI, CNR-ISAC, NUIG, PSI, ULEEDS, UOF, INRNE, CNRS- GAME)

The efforts to further define the natural background aerosol and geographic differences in INP and CCN have taken two approaches. In the first approach (modelling), ULEEDS has expanded on a publication in late 2014, which discussed the 'Occurrence of pristine aerosol environments on a polluted planet' (Hamilton et al. 2014). In this paper, they suggested that pristine areas (i.e. those where current day CCN concentrations are within 20% of pre-industrial) rarely occur outside the poles or the southern hemisphere oceans. This finding in the process of being published in a new manuscript (Carslaw et al. 2016), which suggests that conditions similar to pre-industrial (the year 1850) occur only well downwind from continental landmasses, at least when considering Black Carbon mass, total particle number or CCN number concentrations, and provides an estimation of aerosol, CCN and Black Carbon (BC) concentrations in 1850. In terms of the geographical distribution of INP, ULEEDS has also produced a paper modelling the predicted INP concentration due to desert and oceanic sources (Vergara-Temprado et al. 2016). This suggests that the global maxima of INP concentrations are over and downwind from deserts, with moderate concentrations over the oceans and minima furthest from the oceans and deserts – the poles, tundra regions and central Andes.

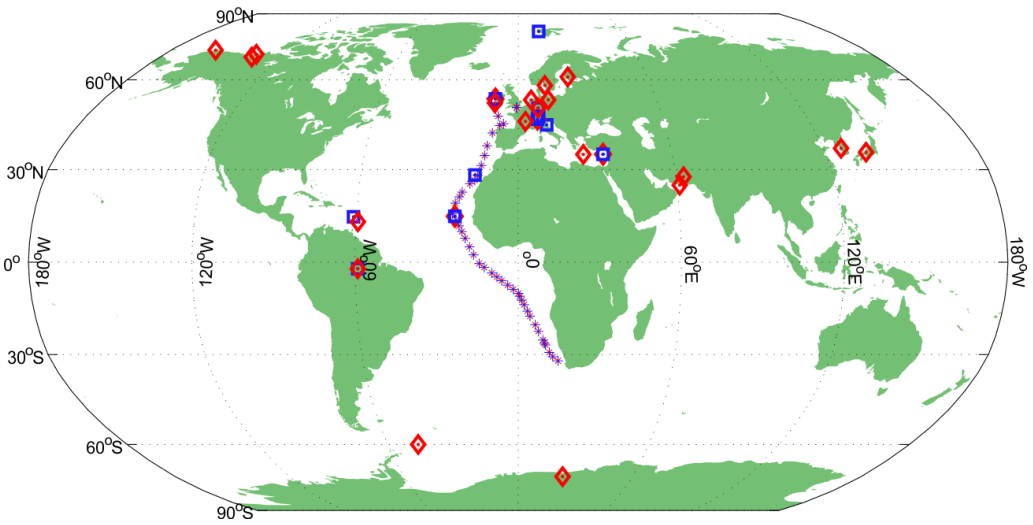

Figure 1.1 Summary of the BACCHUS fieldwork locations. Red locations are CCN measurement sites, blue are INP sites. The map includes new fieldwork locations, which have been contributed to BACCHUS by partners, including fieldwork not directly funded by BACCHUS.

The second approach to compiling the natural background and geographic differences is to review and make additional measurements. These additional observations have concentrated on more remote areas such as mountainous, forest, island or oceanic locations. These locations were chosen for at least one of three purposes – to continue an existing measurement climatology, to measure at a new location, or to measure an area thought to be representative of the natural background. Figure 1.1 summarises the locations of fieldwork contributed to date by BACCHUS Partners and BACCHUS collaborating Institutions.

1.1 BACCHUS Intense INP Observation Periods

During the 18 months covered by this deliverable there have been two intense INP observation periods, one in Mace Head, Ireland (Aug. 2015, hosted by NUIG) and one in Cyprus (Mar. 2016, hosted by CYI)

1.1.1 Mace Head, Ireland

In August and September 2015 ETHZ, CNR-ISAC and ULEEDS, along with a representative of the Kreidenweis Research Group (Department of Atmospheric Science, Colorado State University, USA, abbreviated to CSU), gathered at the Mace Head observatory on the western coast of Ireland, hosted by NUIG. The Mace Head site is ideally positioned to observe the Northern Atlantic natural background aerosol, as the nearest landmasses upwind of the prevailing wind are the direct routes from Northern and Southern America and the circuitous route from Western Africa via the central Atlantic. To facilitate this, NUIG operates a system, which can disable sampling when conditions (wind direction and BLACK CARBON concentration which is used as a proxy for pollution) suggest the air mass is not oceanic. As well as the INP measuring instruments (ETHZ: the HINC-EVAP continuous flow diffusion chamber; CSU, ULEEDS and CNR-ISAC: filter measurement systems), NUIG also provides a plethora of supporting measurements: size segregated CCN (NUIG); aerosol chemistry (HR-ToF-AMS, NUIG) and physics (SMPS, CPC, NUIG), meteorological data (NUIG); airborne Unmanned Aerial Vehicles (UAVs) (radiosonde, vertical distribution, updraft at cloud base (T, RH, p, Td, LCL, wind, Wb, Np (Dp > 300nm) SS, CNRM); ground based remote sensing (NUIG). The INP measurements from this campaign are, or will be, available in the BACCHUS database; the CCN measurements form part of a long-term measurement set and will be added to the ACTRIS database. Publication of the campaign as a whole is under preparation as a two-part manuscript co-lead-authored by James Atkinson (ETHZ) and Christina McCluskey (CSU).

1.1.2 Cyprus

Since January 2005 at the regional background site of Agia Marina Xyliatou (35°02’19"N, 33°03’28"E, 532 m asl), CYI has operated the Cyprus Atmospheric Observatory (CAO; http://www.cyi.ac.cy/index.php/cao.html). Measurements have been intensified during BACCHUS and focus on continuous observations of aerosol properties (chemical composition, size distribution, optical properties) while complying with the standard operation procedures of ACTRIS. The results accumulated during BACCHUS have been used to characterize the ambient background aerosol of Cyprus. In the frame of the FP7-BACCHUS and H2020 – ACTRIS2 project, CYI has developed the Unmanned Research System Laboratory (USRL, **Error! Reference source not found.** left; http://www.cyi.ac.cy/index.php/usrl.html) which operates a unique fleet of UAVs from a private runway near CAO, flying within a large and private air space allocated permanently by the Civil Aviation Authorities up to 3 km asl. Measurements performed using UAVs provide vertical in-situ observations, which are crucial when investigating long-range transported aerosols layers and their interactions with clouds. Located in the vicinity of the two largest deserts in the world (Sahara, Arabic Peninsula), Cyprus represents a strategic location to investigate the role of dust aerosols on INP concentrations and properties. With the objective to build a robust INP database representative of dusty environments, two major BACCHUS field campaigns have been organized at CAO in Spring 2015 (March) and 2016 (April). This period of the year is usually highly impacted by dust storms.

During both campaigns, efforts were put into building a comprehensive aerosol database composed by a suite of ground-based INP observations, remote sensing (Lidar, sunphotometer)

located in Limassol (Cyprus University of Technology) and Nicosia (The Cyprus Institute), and intensive UAV aerosol observations with up to 50 INP samples taken below/above the boundary layer top in 2016. UOF was responsible for UAV INP measurements using the FRIDGE INP counter, with samples analysed by UOF at CYI. In addition to the deposition/condensation INP measured routinely we also measured immersion INP by filter collection and droplet freezing. During 43 individual flights deposition/condensation mode INP were successfully sampled and analysed immediately (**Error! Reference source not found.** right). The campaign encountered several episodes of dust transport from North African sources that are well reflected in the INP and in the aerosol data. The vertical profiles indicate that the major transport of dust and INP occurred at several km above ground. A manuscript discussing the vertical profile data is in preparation (Schrod et al. 2016), and the data will enter the BACCHUS data base before 12/2016.

Additionally, during both intensive campaigns ground based CCN and INP measurements were performed at CAO by various teams (CNRS-LaMP, CNRS-CNRM, ETHZ, TROPOS, INUIT consortium). During the 2015 campaign, CN/CCN size distribution measurements were performed and the influence of nucleation on CCN was then investigated. INP measurements were also performed by ETHZ using the HINC instrument. During the April 2016 campaign further INP instrumentation, TROPOS (filter measurements), ETHZ (liquid impactor measurements plus the HINC instrument) and instrumentation provided by the INUIT consortium, expanded the capabilities of measuring INP during BACCHUS.

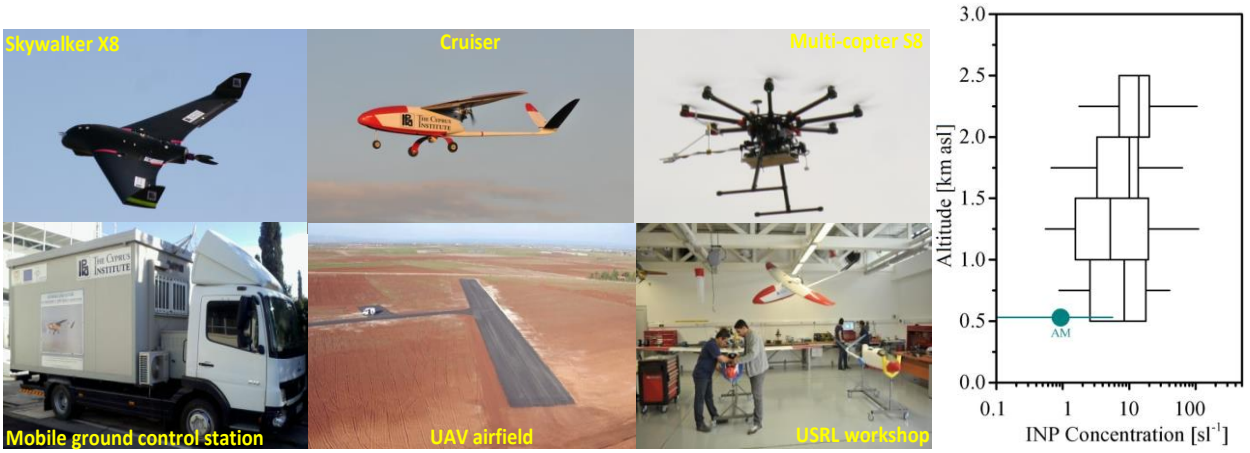

Figure 1.2. Left) The equipment and facilities of the UARL of CYI. Right) Vertical profile of deposition/condensation INP at -30°C measured by UOF over Cyprus, median (central line in box), interquartile (box) and full range (black bars) of INP number concentration. AM denotes the concentration observed at the ground site.

1.2 CCN Observations

Outside of the intense observation campaigns, there has been work on additional CCN observations. The largest effort has been performed by PSI, who is leading the community effort to synthesizing collocated CCN (see deliverable D2.4), particle number size distribution and chemical composition data from observatories in Europe, North America and Asia (**Error! Reference source not found.**).

CCN number concentrations alongside with submicrometer particle number size distributions and particle chemical composition have been measured at atmospheric observatories of the Aerosols,

Clouds, and Trace gases Research InfraStructure (ACTRIS) as well as other international sites over multiple years. PSI harmonized data records from 11 observatories, spanning 98,677 instrument hours for CCN data (> 11 years), 157,880 for particle number size distributions (> 18 years), and 70,817 for chemical composition data (> 8 years). The observatories represent nine different environments, e.g. Arctic, Atlantic, Pacific and Mediterranean maritime, boreal forest, or high alpine atmospheric conditions. This is a unique collection of aerosol particle properties most relevant to studying aerosol-cloud interactions, which constitute the largest uncertainty in the anthropogenic radiative forcing of the climate. The dataset is appropriate for comprehensive aerosol characterization (e.g. closure studies of CCN), model-measurement comparisons and satellite retrieval method evaluation, among others. Data have been acquired and processed following international recommendations for quality assurance and have undergone multiple stages of quality assessment. The data are available via the ACTRIS database EBAS (http://actris.nilu.no/Content/Products) and the respective data descriptor manuscript has been submitted in September 2016 (Schmale et al. 2016).

Further new CCN observations have been made by BACCHUS partners. These include the PEGASOS ship campaign, which occurred in the Weddell Sea close to the Antarctic Peninsula in Jan.-Feb. 2015, during which NUIG performed CCN and aerosol size distribution measurements for which data analysis and validation is in progress. CCN measurements have been undertaken at three sites (Taunus Observatory near Frankfurt, Germany, 2013-2014; ATTO site, Amazon, Brazil since Mar. 2014; Barbados since Aug. 2016) under the coordination of MPI-C. These sites cover different environments, from a rural forest near a large city (Taunus), to a tropical rainforest remote from major population centres (ATTO Brazil) and an oceanic location (Barbados). Observations at the ATTO site have been documented (Pöhlker et al. 2016), while data from the other two sites are still under-going analysis. A new method, the broad supersaturation scanning (BS2) approach, was also developed for rapid measurement of aerosol particle hygroscopicity and cloud condensation nuclei activity (Su et al. 2016).

CCN measurements by TROPOS on the research vessel RV *Polarstern* cruising the Atlantic from South Africa to Germany show a dependence of the CCN number concentration on the air mass origin. The occurrence of clean marine aerosol comes along with a generally low CCN concentration, typically below 100 particles per cm^3. However, continental influenced air masses show CCN number concentrations up to 1000 particles per cm^3. This variability can also be seen in the CVAO CCN data, which shows a distinct increase during Saharan dust events. Further TROPOS CCN measurements in the Arctic and Antarctic have been performed in North Canada (Inuvik and Tuktoyaktuk) in spring 2014 and at the Princess Elisabeth Antarctica Research Station

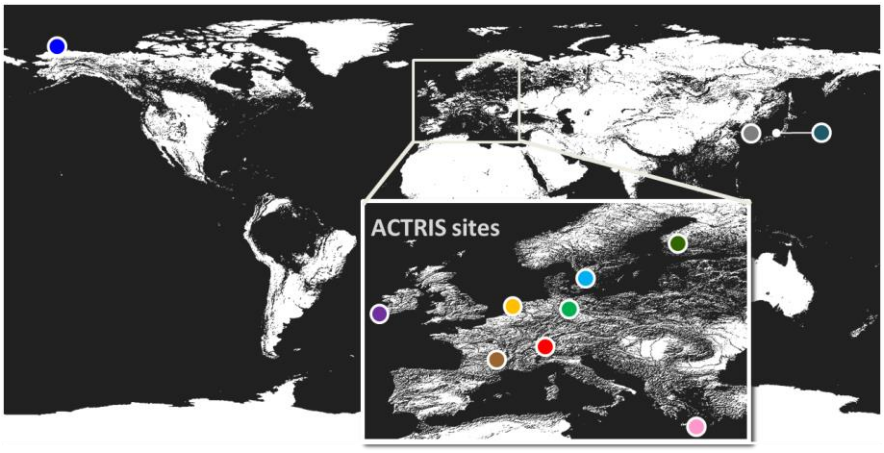

Figure 1.3. Locations of the CCN observation sites covered by the PSI led synthesis.

during the Antarctic summer 2013/2014. These measurements are all still undergoing analysis in preparation for publication and database submission.

In Finland, CCN measurements have continued at the two FMI sites Puijo (near Kuopio) and Pallas (north of Helsinki). These sites represent the continuation of long-term measurements while also providing a comparison between the semi-urban Pallas site and the rural/forest Puijo site. Measurements from these sites were most recently published in 2015 (Paramonov et al. 2015); further publications are currently being worked on and submission of the data to the ACTRIS database is planned.

1.3 INP Observations

As well as Mace Head and Cyprus, additional INP concentration measurements have been made at, and analysis worked on for, several other sites during BACCHUS. From CNR-ISAC, campaigns took place between 2014 and 2016. They are reported in section 2.3. Datasets of the campaigns have been delivered to the BACCHUS database. The last database (Capogranitola) will be delivered at completion of the analysis.

UOF has continued to monitor the number concentration of deposition/condensation INP by sampling at four surface sites (Table 2.1) and analysing these samples in the lab at Frankfurt (see section 2.5). All 1085 samples collected so far have been analysed; the images of these samples are currently reprocessed. The preliminary data will be submitted to the database by the end of 2016. Sampling will continue until the end of 2016, and these samples will be processed and data reported in 2017.

TROPOS performed INP concentration measurements with the continuous flow diffusion chamber SPIN during two intense campaigns from Oct. – Dec. 2015 on RV *Polarstern* (cruise PS95) and during the 2016 dust season (Jan. – Feb.) at the Cape Verde Atmospheric Observatory (CVAO) on Cape Verde Islands. The PS95 cruise from Bremerhaven to Cape Town offered the opportunity to probe a geographical cross section from 54° N to 35° S for the regional IN concentrations. The variability in INP concentration with geographic position and nucleation temperature gives a hint on the sources of INP, active at different conditions and in different regions. Error! Reference source not found. shows 30min averages of INP concentrations measured at -36 °C and -32 °C. Depending on the experimental temperature, different sources contribute to the active INP population. For example a clear influence of the Saharan desert dust outflow between the Canary Islands and Cape Verde can be seen at -32 °C. In addition to the desert dust, the continental aerosol from Europe and South Africa was observed to be an important source for INP at -36 °C. These local sources seem to enhance the INP concentration mainly at low temperatures while little effect is observed on the INP concentration at higher temperatures.

While the PS95 data cover a large geographical space, SPIN measurements at CVAO provide information on the temporal variability in INP concentration at a fixed position. CVAO is located in the subtropical marine boundary layer where besides marine sources, aerosol transported from the Saharan desert, the Sahel zone and SW Europe are the main contributors of aerosol.

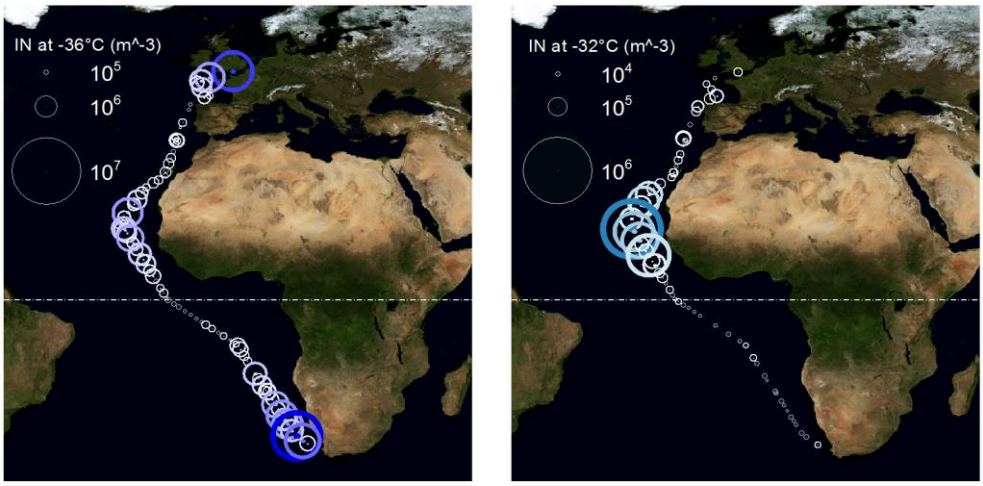

Figure 1.4. INP concentration measured during PS95 at -36 °C, -32 °C and 105 %RH_w. Circle areas are scaled with INP concentration and coloured according to the number of INP. Note that the circle size is scaled by a different factor in each subfigure and INP concentration corresponding to circle area is indicated in each figure separately.

SPIN measurements have a high temporal resolution and cover the low temperature regime (233 K < T < 248 K). To extend the dataset to the concentration of rare INP active at high temperatures (T > 258 K), PM10 filter samples are analysed using a drop freezing technique. This way, time series of INP concentrations in the immersion mode are determined on a 1-3 day resolution, re-using PM10 filter samples collected at CVAO since 2008. The same technique was used to probe daily filter samples collected during the 2016 BACCHUS campaign on Cyprus. Data from all campaigns are available in the BACCHUS INDB (see section 1.3.1), except for the CVAO filter measurements, which are still being analysed.

As well as attending both of the Intense INP Observation Periods, ETHZ has produced and documented several INP observation campaigns within the framework of BACCHUS. Measurements were made on the island of Tenerife (Canary Isles, Spain) during 2013-2014 and were recently documented (Boose et al. 2016a). Observations are on-going at the High Altitude Research Station Jungfraujoch, Switzerland with measurements during 2012-2014 recently documented (Boose et al. 2016b,) and publication of measurements 2014-2016 is in preparation. Analysis is also nearly completed on measurements made at a semi-rural Zurich site in 2014, with documentation expected during 2017. Data from all these campaigns (pre- and post-publication) is available in the BACCHUS INDB.

1.3.1 INP Database

To enable compilation of a geographical dataset of INP concentrations, collection of new and historical data continues. Currently the BACCHUS INP Database (INDB, http://www.bacchus-env.eu/in/) contains 67 searchable records, of which 46 have data files available for direct download. The database is freely available for scientists though a web-portal upon completion of a data protocol. The locations covered by data in the INDB are shown in Figure 1.5. Except for a scattering of historical data, most regions lack significant data density – Central Europe and the USA are well covered (data around Australia dates from the early 70's). The majority of data collected to date during BACCHUS is available for download. Documentation of the database and a review of all the available data is under preparation and will be published in 2017.

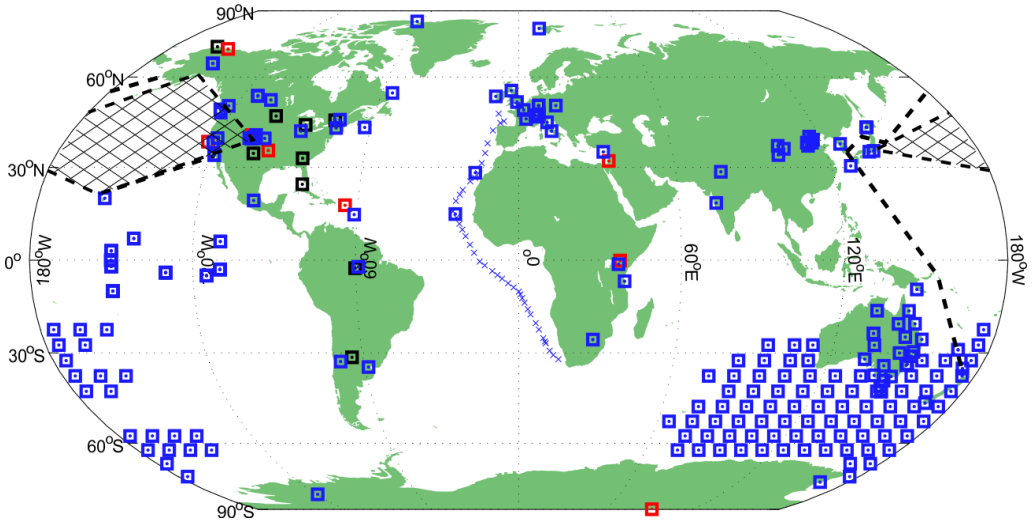

Figure 1.5. Geographical distribution of data in the BACCHUS INDB per the end of Oct. 2016. Blue data is available for direct download, red data is searchable but must be acquired from the data owner, and black points denote known campaigns, which do not currently appear in the database. Much of the data outside of Europe and Northern America dates from campaigns pre-1990, particularly those around Australia.

2. Contribution from task 1.3 "Quantification of natural (biological and dust) and anthropogenic contributions to INP" (MPI, CNR-ISAC, UOF, Colorado State University)

2.1 Database for bioaerosols and modelling of relevant species acting as INP. (MPI)

In this task, we summarize on-line measurements of bioaerosols by UV-APS (ultraviolet aerodynamic particle sizer) and WIBS (wideband integrated bioaerosol spectrometer) all over the world. We have now established a database to collect measurement data via the FTP server (ftp.mpic.de). Currently, we have collected bioaerosol information from the following campaigns: Mainz 2008; Amazon 2008; Hyytiälä, Finland 2009; Killarney National Park, Ireland 2010; Karlsruhe, Germany I 2010; MEGAPOLI Study (Paris, France) II 2010; BEACHON Study (Colorado, USA) 2011; Karlsruhe, Germany II 2011; Mainz II 2011; Beijing 2013; Xiamen 2013; Nanjing 2013 (Yu et al. 2016); ATTO 2014-2016. For each campaign, the measurement description (e.g., location, season and site category) and data (number concentration and size distribution of total aerosols and bioaerosols) are provided. The BACCHUS Bioaerosol Database Protocol is developed based on the general BACCHUS Database Protocol to regulate the data exchange and is briefed as follows: (1) Data will be stored at MPIC, data submission will be coordinated by Zhibin Wang from Max Planck Institute for Chemistry (zhibin.wang@mpic.de) and Alex Huffman from University of Denver (Alex.Huffman@du.edu). (2) Data providers reserve all rights of their data. (3) Data access is limited to the BACCHUS project and external users, who have signed the data protocol. Any transfer/usage of data stored in the database must be approved by the data providers on a case-by-case basis. Especially when data are used in publications, joint authorship must be offered and intellectual input must be discussed with the data owner and scientists who have contributed substantially to data processing (such as synthesis or merging of datasets in addition to that carried out by the data provider). The FTP server also documents modeling results of aerosol species that are relevant for atmospheric IN.

2.2 Long-term aircraft measurements of Black Carbon (MPI)

Since August 2014, continuous Black Carbon measurements within the upper troposphere and lowermost stratosphere (UT/LMS) are performed in the framework of the IAGOS-CARIBIC research project (contact person: Yafang Cheng, yafang.cheng@mpic.de). The CARIBIC-BLACK CARBON measurements are done beside greenhouse gas and aerosol measurements with a special instrumented airfreight container located in the cargo bay of a German Lufthansa aircraft. Measuring on a monthly basis leads to more than 600 hours of Black Carbon measurements over four continents. Our measurements provide size-resolved Black carbon concentration as well as the coating thickness.

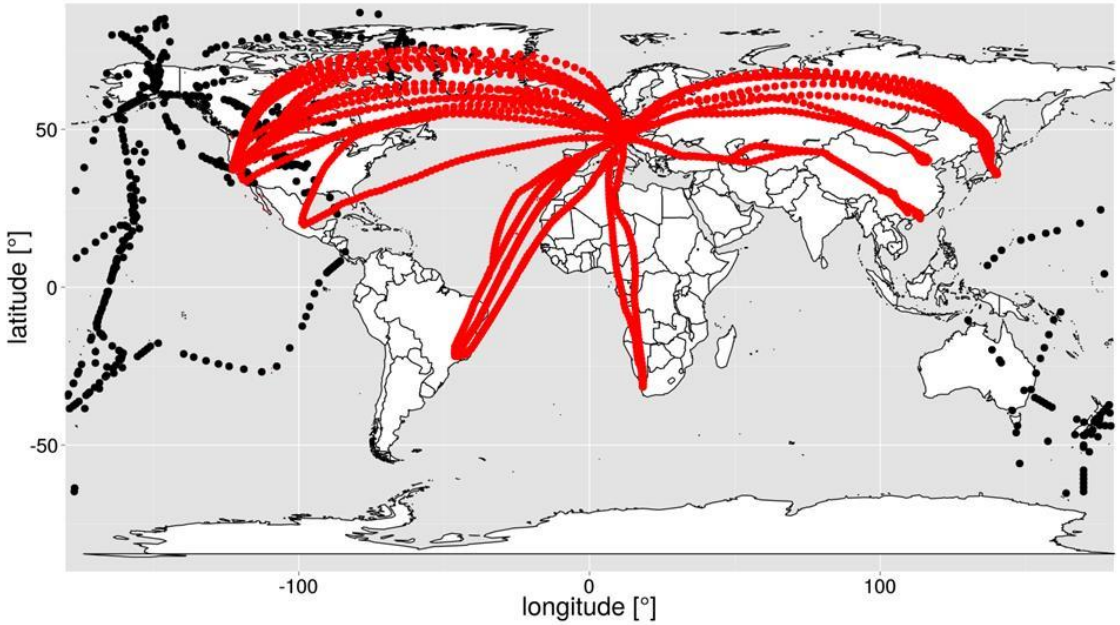

Figure 2.1. Aircraft measurements of Black Carbon aerosols in CARIBIC-BLACK CARBON project. The red dots mark the flight routes. The black dots mark Black carbon measurements above 8 km obtained during the HIPPO and ARCTAS campaigns.

2.3 New INP measurements (CNR-ISAC)

Six experimental campaigns concerning measurements of INP concentrations were carried out by CNR-ISAC in the framework of the BACCHUS Project. The campaigns took place between 2014 and 2016, at the following sampling sites:

- San Pietro Capofiume (SPC), a rural background site, near Bologna (Italy) in the Eastern Po Valley, in the periods 10 - 21 February (SPC1) and 19 – 30 May 2014 (SPC2);
- Monte Cimone (MC) Global Atmospheric Watch (GAW) station, a high altitude site (2165 m asl) in the Apennine Mountains facing the Po Valley, in the periods 19 – 29 May 2014 (MC1, in parallel with SPC2) and 05 – 12 October 2015 (MC2);
- Mace Head (MH), a North Atlantic coastal site in Western Ireland, during August 2015, with the aim of investigating the dominant sources of INP in the North Atlantic Marine Boundary Layer;
- Capogranitola (CG) a background coastal site facing the Strait of Sicily.

Samples were collected using a parallel PM1 - PM10 sampling system and were processed in a dynamic filter processing chamber (DFPC), housed in a refrigerator, that was used to detect and determine the concentration of INP, at different temperatures and supersaturations with respect

to ice and water (Santachiara et al., 2010). Measurements with the DFPC below water saturation ($S_w < 1$) are considered representative of deposition nucleation, while above water saturation ($S_w \geq 1$) of immersion- and condensation-freezing. In detail, measurements were carried out at -22°C (filters sampled at MH) and -18°C (other sites), with $S_w = 0.96$ and $S_w = 1.02$.
The campaigns held at SPC and MC are representative of continental background conditions, characterized by high anthropogenic emissions (traffic, wood burning, industry and agriculture). Moreover, episodes of Saharan dust transport have been observed in each of these campaigns. On the other hand, sampling at MH was performed in strictly selected unperturbed marine air masses from the North Atlantic Ocean and is representative of natural INP emitted from the ocean. Figure 2.2 shows an overview of the INP concentrations observed at the different sites for PM1 and PM10 aerosol size fractions (analyses of the CG samples are still ongoing). The lower average concentration in the PM10 fraction was measured at MH (10 m^{-3}) and the highest at SPC (310 m^{-3}, during SPC1).

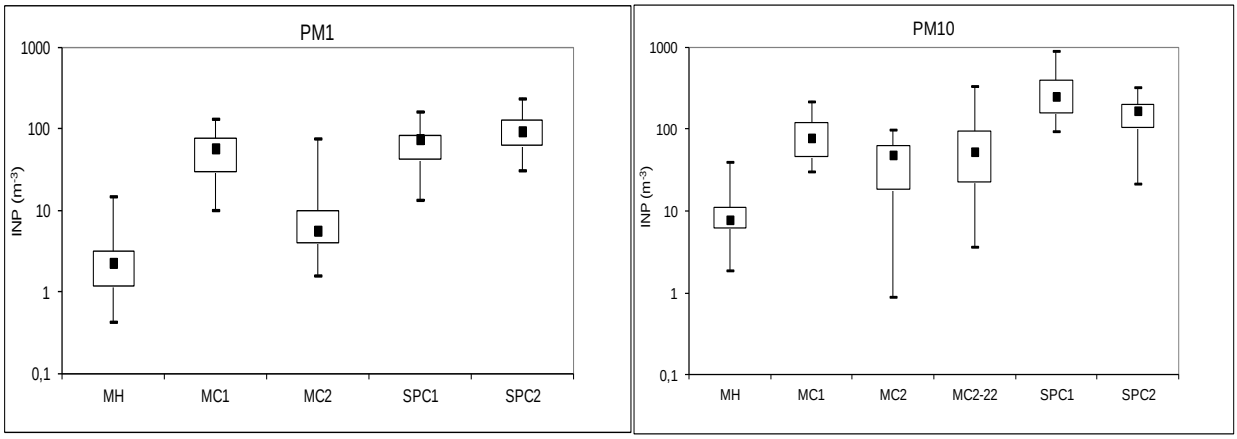

Figure 2.2. INP concentration (m^{-3}) at the different sites in the PM1 (left) and PM10 (right) size ranges. MC2-22 indicates the results of PM10 filters analysed at -22°C instead of -18°C.

Datasets of the campaigns SPC1, SPC2, MC1, MC2 and MH have been delivered to the BACCHUS database. The last database (CG samples) will be delivered at completion of the analysis.

2.4 Mace Head Observatory measurements of ice nucleating particles (Colorado State University: C. S. McCluskey, P. J. DeMott, T. C. J. Hill)

Measurements of INPs were taken at the Mace Head Observatory from 6 to 27 August 2015 during the BACCHUS ice nucleation measurement comparison campaign. Two aerosol filters, CLEAN and ALL, (Pre-sterilized Nuclepore^{TM} track-etched polycarbonate membrane filters (47 mm diameter, Whatman, GE Healthcare Life Sciences, Piscataway, NJ) with a pore size of 0.05 µm) were collected each day at the top of the 10 meter mast; total sample collection periods ranged from 6 - 37 hrs (20 hrs on average). The pump for the CLEAN filter was powered using the MHO Clean Sector Sampler (Rinaldi et al., 2009), which powers the pump for clean-sector (Black Carbon < 15 ng/m^3; wind direction 180º to 300º). The pump for the ALL filter was powered continuously during the total collection period. The CLEAN filters represent INPs from pristine marine aerosol and the ALL filters represent INPs from both marine and terrestrial aerosol particles. If filters were visibly wet from rain or mist, they were discarded. Five blank filters were also

collected to evaluate contamination from collection/shipping process. Filters were kept frozen (-20 °C) during the study and shipped to CSU on dry ice.

The CSU Ice Spectrometer (IS, Hiranuma et al., 2015) was used to determine number concentrations of immersion freezing INPs (n_{INP}, per L of air) active at temperatures 0 to -27 °C. Filters were immersed in 7 mL deionized water (18 MΩ, 0.2 µm pore filtered and, further cleaned by passing through an 0.02 µm pore Anotop syringe filter (Whatman)) and shaken for 20 minutes. Aliquots (50 µL) of sample solution were dispensed in wells (n=24 or 32) of a PCR tray (µCycler; Life Science Products, Frederick, CO), which were placed into aluminum blocks of the IS. A chiller was then used to cool the blocks from 0 to -25 °C at -0.33 °C min^{-1}, and the number of wells frozen was recorded every 0.5 or 1 °C. Number concentrations of INPs per volume of liquid are determined as a function of temperature based on $-\ln(f)/V_a$, following Vali et al. (1971), where f is the fraction of unfrozen aliquots and V_a is an aliquot volume. Computation of n_{INP} is then obtained from the total volume used for rinsing and the volume of air collected.

Additional treatments to sample solutions were performed, including 1) heating at 98 °C for 20 minutes 2) digestion by hydrogen peroxide and 3) size filtering (various pore sizes). Post treated sample solutions were then analyzed in the IS.

Each sampling period will have n_{INP} temperature spectra corresponding to a set of CLEAN & ALL filters. On some days, conditions for the clean sector were not met and thus do not have CLEAN filters. Various treatments were performed on most days, depending on trends in n_{INP} and aerosol chemistry provided by the aerosol mass spectrometer. Basic analysis will be completed by 28 October 2016 and treatment analyses will be completed by January 1, 2017. Data availability follows BACCHUS data protocol.

2.5 New measurements of ice nucleating particles (UOF)

We continued to monitor the number concentration of deposition/condensation INP by sampling at four surface sites (Table 2.1). More details are given in section 1. In 2016 we participated in the joint BACCHUS/INUIT field experiment in Cyprus. During 4 weeks of April daily samples were collected at Agia Marina Station (35°02'19"N, 33°03'28"E, 532 m asl). The FRIDGE INP counter was deployed to Cyprus, and samples were analyzed on site. In addition to the deposition/condensation INP measured routinely we also measured immersion INP by filter collection and droplet freezing. Miniaturized sampling systems were adapted and integrated into two Unmanned Aerial Vehicles operated by CYI. During 43 individual flights deposition/condensation mode INP were successfully sampled and analyzed immediately. The campaign encountered several episodes of dust transport from north African sources that are well reflected in the INP and in the aerosol data. The vertical profiles indicate that the major transport of dust and INP occurred at several km above ground. A manuscript on the vertical profile data will be submitted in October, and the data will enter the database before 12/2016.

Table 2.1. Details of the UOF sampling periods

Site	Coordinates	Sampling frequency	No Samples	Sampling period
Svalbard (Spitsbergen)	78°54'29"N, 11°52'53"E	1 per 2 days	328	7-12/14, 5-12/15, 1-6/16
Martinique	14°44'05"N, 1°08'48"W	1 per 2 days	218	8-9/14, 5-12/15, 5-6/16

Amazonian Tall Tower	2°8'48"S, 59°0'18"W	1 per 2 days	133	8-9/14, 5-7/15, +50 resting at site
Taunus Observatory	50°13 N‘, 8°27‘ E	1 per 2 days	406	1-12/14, 5-12/15, -8/16

In cooperation with BACCHUS partner University of Gothenburg (Erik Thomson and Jan Pettersson), we performed field observations at the sea port of Gothenburg. From the measurements of aerosols and INP in 83 ship plumes during two campaigns at Gothenburg, that were organized and conducted by University of Gothenburg, a significant emission of INP by ships was established. Emission factors were derived. A manuscript considering the impact of growing arctic IN emission from shipping is in preparation. 50 aerosol samples that had been collected in summer 2015 by E. Thomson from the free troposphere at the GAW station on Mt. Kenya have been processed and the results are currently being evaluated.

3. Contribution from task 1.4: “Quantification of the biogenic and anthropogenic contribution to organic aerosol and their ability to act as CCN” (CNR-ISAC, NUIG, UHEL, CNRS-GAME, CYI, UOC, MPI-C, PSI, FMI, IRNE)

Task 1.4 includes analysis/re-analysis of long-term CCN and chemical datasets from European observatories.

3.1 Rationale

The complexity of the mixing state of aerosol compounds in submicron particles challenges the same concept of “source apportionment of CCN” (and in general of aerosol *number* concentrations). In the absence of direct measurements of the chemical composition and mixing state of CCN in their full size spectrum, we focus our analysis on the phenomenology of CCN with concomitant chemical observations by state-of-the-art online instrumentation (mainly AMS technologies). Aerosol chemical measurements through AMS or ACSM are representative mainly of accumulation mode aerosols, with a partial overlap with CCN populations for the low supersaturation (*S*) regime, but certainly not with CCN at high *S* values which are largely accounted for by ultrafine particles. Moreover, AMS measurements do not provide information of the mixing state. However, the recent progress on nascent ultrafine particles has shown that the same low-volatility compounds take part in the growth of both ultrafine and accumulation mode particles (Riipinen et al., 2011). The generation of CCN and accumulation of particle mass are therefore affected by the availability of the same pool of condensable products, although the relationship between the two processes is certainly non-linear (with some negative feedbacks, e.g., through condensation sink effects) and controlled by other variables. The usefulness of the phenomenology of joint CCN – aerosol chemical compounds frequency distributions presented in this study is mainly in providing constrains to CTMs, especially with respect to testing schemes of secondary aerosol formation and growth.

3.2 Data sets

Observations are available from CCN counters, Aerosol Chemical Speciation Monitors (ACSM) (or Aerosol Mass Spectrometers, AMS) and Particle Soot Absorption Photometer (PSAP) (or Multi-Angle Absorption Photometer, MAAP, or aethalometers) at the following ACTRIS rural stations: Jungfraujoch (JFJ), Mace Head (MHD), Finokalia (FIK), Hyytiälä (SMR), Melpitz (MPZ), Cabauw (CBW), S. Pietro Capofiume (SPC). The datasets encompass long-term (> 1 year)

observation records, with the exception of SPC, which is based on an intensive field study, and it is included here mainly to represent as an extreme for the polluted conditions (in "European terms"). Table 3.1 summarizes the database.

Table 3.1 Available field observations

Station	CCN supersaturation levels	Online chemistry	BLACK CARBON measurements	Time coverage of CCN measurements	number of concomitant CCN, AMS and BLACK CARBON hourly measurements
Jungfraujoch (JFJ)	0.10 ,0.15 ,0.20, 0.25, 0.30, 0.30, 0.40, 0.50, 0.70 ,1.0	ACSM	1.1.1.aethalometer	July 2012 – July 2013	3500
Mace Head (MHD)	0.10, 0.25, 0.35, 0.50, 0.75, 1.0	AMS	aethalometer, MAAP	July 2011 – April 2012	1074
Finokalia (FIK)	0.2, 0.4, 0.8, 1.0	ACSM	aethalometer	Nov 2014 – Oct 2015	5361
Hyytiälä (SMR)	0.10, 0.20, 0.30, 0.50, 1.0		PSAP 3W	May 2012 – Dec 2014	4139
Melpitz (MPZ)	0.10, 0.20, 0.30, 0.50, 0.7	ACSM	MAAP	Jan – Dec 2013	11380 (2268 at the single SS levels)
Cabauw (CBW)	0.10, 0.20, 0.30, 0.50, 1.0	ACSM	PSAP	Oct 2012 – April 2014	3297
S. Pietro Capofiume (SPC)	0.2, 0.4, 0.6, 0.8, 1.0	ACSM	MAAP	Feb 2014	501

CCN data originate from polydisperse CCN counters, with the exception of the counter at MPZ, which is monodisperse. Polydisperse CCN distributions from MPZ were reconstructed by integrating the CCN concentrations over the 20 and 260 nm particle diameter range for each *S* level.
Black Carbon concentrations were derived from aerosol extinction measurements (in Mm^{-1}) by applying a MAC of 10 g m^{-1}. All data were averaged to an hourly time resolution.

3.2.1 CCN concentrations and pollution "regimes"

Model studies suggest that CCN concentrations are not expected to increase linearly with anthropogenic emissions. This dependence can be rather visualized by a concave curve with larger increases of CCN at small increases of pollution levels and by smaller increases between moderately polluted and very polluted conditions (Carslaw et al., 2013). Tendency of "saturation" at high anthropogenic emissions can be due to the suppression of nucleation in presence of high condensation sinks. We have investigated the way CCN concentrations are associated with increasing levels of pollution at the ACTRIS stations. We used the atmospheric concentration of Black Carbon as a proxy for pollution. Figure 3.1 reports CCN concentrations as a function of

Black Carbon loadings in a log-log plot. The range of variation represents the variability (1st and 3rd quartiles) of CCN within small intervals of concentrations of Black Carbon (24 bins in the whole range, spaced by a factor of 1.5).

Figure 3.1 exemplifies the variability of CCN concentrations as a function of Black Carbon at a low SS (0.2%, top) and a high SS (1%, bottom) for remote (left) and polluted rural stations (right). Regression lines for most of the curves show positive slopes lower than 1 in log-log scale, which correspond to a concave curve using a linear scale. This is especially true at the high *S* level. The most evident exception is for the MHD dataset, where the increase of CCN concentrations with Black Carbon is linear or superlinear, showing no saturation effects at high Black Carbon levels. At small Black Carbon loadings, CCN concentrations tend to flatten out at MHD, which may reflect the existence of a natural background, which is of approx. 100 particles per cm^{-3} at 0.2 % *S* . Finally, it should be noted that the saturation effect on CCN is extreme for SMR at 1% *S*, with very high and virtually constant average CCN concentrations above 30 ng m^{-3} of Black Carbon. If we consider the concentrations of CCN at 10 ng m^{-3} of Black Carbon as representative for the pristine conditions in the boreal forest, then the increase in anthropogenic emissions leads to only a moderate increase in CCN. This is consistent with the fact that new particle formation can occur starting from biogenic compounds at very small or even null concentrations of anthropogenic precursors (SO_2) (Tröstl et al., 2016). In conclusion, if we consider the dependence of CCN concentrations on Black Carbon levels as a direct - experimentally based – estimate of the increase of CCN from pristine to polluted conditions for specific environments (keeping constant land use and biogenic emissions), a marked increase of CCN is observed for the small *S*, while a more complex behavior is found for the remote stations at high *S* values.

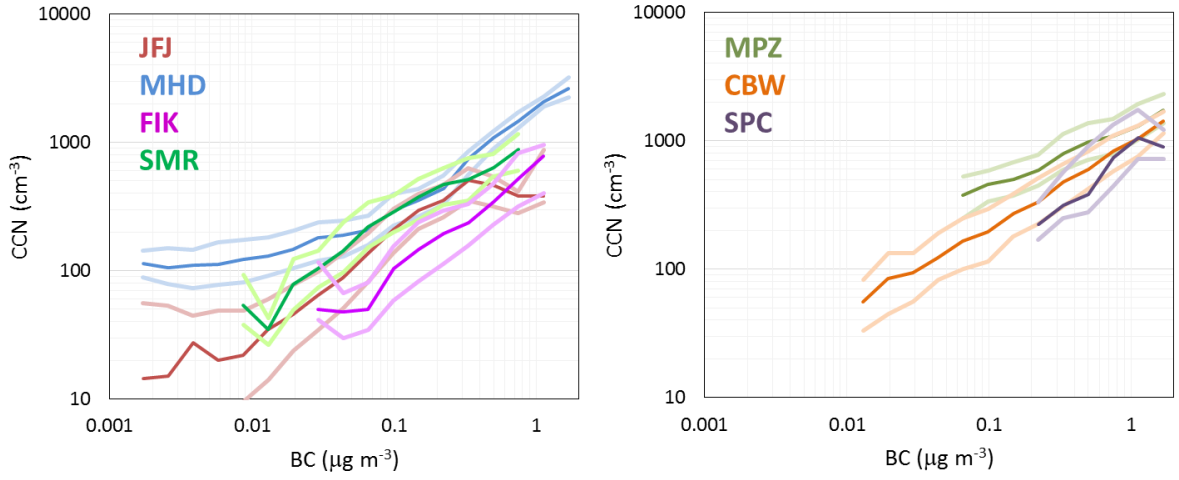

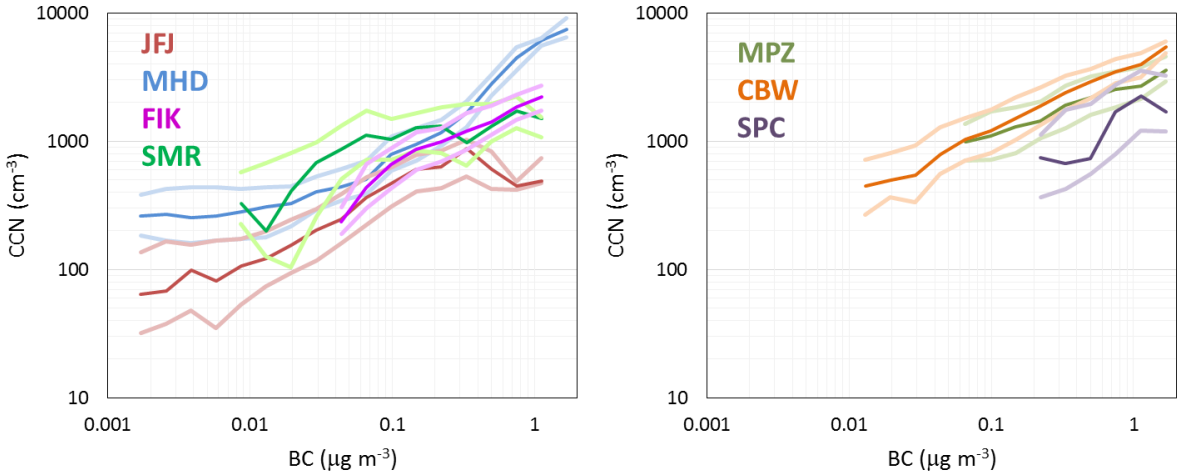

Figure 3.1. CCN concentrations vs BLACK CARBON levels. The figures report statistics for CCN concentrations in 24 intervals of concentrations of BLACK CARBON (dark line: median; light lines: 1st and 3d quartiles). Data for CCN at 0.2% (top panels) and 1% S (bottom panels) are reported. In the case of MPZ, for which data at the 1% S are not available, the CCN at 0.7% S are reported in the bottom panel.

3.2.2 Frequency histograms and contingency tables

The paper by Paramonov et al. (2015) provides already a climatology of CCN at several European (and some extra-EU) sites. Here we extend the climatology to CCN with concomitant aerosol chemical measurements. The intercorrelation between the concentrations of CCN and of aerosol chemical parameters (AMS species + BLACK CARBON) was studied using joint frequency distributions. These are preferred over a simple correlation analysis when the shape of distributions is unknown. Joint frequency distributions can be visualized as 2D histograms, and reported in numerical form as contingency tables. Both representations require the continuous dimension of CCN (or AMS species or BLACK CARBON) concentrations binned into discrete variables. Here ranges of concentrations in a log scale were employed. The number of bins to be used is subject to discussion. Most authors suggest that the number of bins must be proportional to the square root of the number of observations *n*. This has some impact on the present analysis, because the site-specific datasets are of a different size (Table 3.1). The number of histogram columns was then fixed to the square root of *n*, but, since we deal here with a 2D histogram, the number of bins for each of the two variables (in the case of a square matrix) was set to the fourth root of *n* (approximated to the closest integer number). Each of the resulting contingency tables is an I x I square matrix where I = 9 (for CBW, JFJ and SMR), or 8 (for MPZ), 7 (MHD) or 6 (SPC): the resolution of the joint frequency distributions is therefore a direct function of sample size.
. The figures below (Fig. 3.2 to 3.4) show some examples. Most distributions look monomodal (at least with the resolution used here), but not all. Bimodal distributions provide the best opportunity to define “chemical regimes” for CCN. Figure 3.2 (JFJ data for 0.7% *S*) shows a monomodal distribution in the CCN vs. SO4 space (upper panel) and a bimodal distribution in the CCN vs OM (organic matter) space (lower panel). When splitting the histograms into two regions - for the high and the low concentrations of SO_4 or OM - and integrating the corresponding CCN frequency distributions, we obtain the plots on the right, which can be viewed as the conditional probability of CCN to occur at given ranges of concentrations of SO_4 or OM. The distributions of CCN concentrations for high and low SO_4 concentrations exhibit a larger overlap between each other than in the case of CCN vs high and low OM concentrations (especially in the range of CCN

concentrations between 150 and 300 cm^{-3}). The concentrations of CCN at 0.7% *S* appear to correlate less with the concentrations of sulfate than with the concentrations of OM at JFJ. The reasons can be multiple. Being a mountain site, a certain fraction of the variability in the aerosol concentrations is triggered by the planetary boundary layer (PBL) meteorology. Apparently, sulfate is better vertically mixed than OM or CCN.

CCN concentrations at moderate SS levels (0.3%) appear less correlated with SO_4 than with carbonaceous aerosols (Black Carbon) also at some low-altitude stations (CBW, Figure 3.3) indicating that the PBL meteorology is not the only explanation (or not everywhere) for such behaviors.

In general, the degree of statistical correlation between the concentrations of CCN and those of AMS/ACSM chemical compounds varies substantially between stations. They can correlate very coarsely like in the case of CCN and NO_3 in the Po Valley (Fig. 3.4, left), which is expected: particulate NO_3 is enriched mainly in large accumulation mode particles and contributes to a very small extent to ultrafine particle formation and growth. On the other hand, NO_3 concentrations correlate well with CCN at another polluted station, CBW (Fig. 3.4, right).

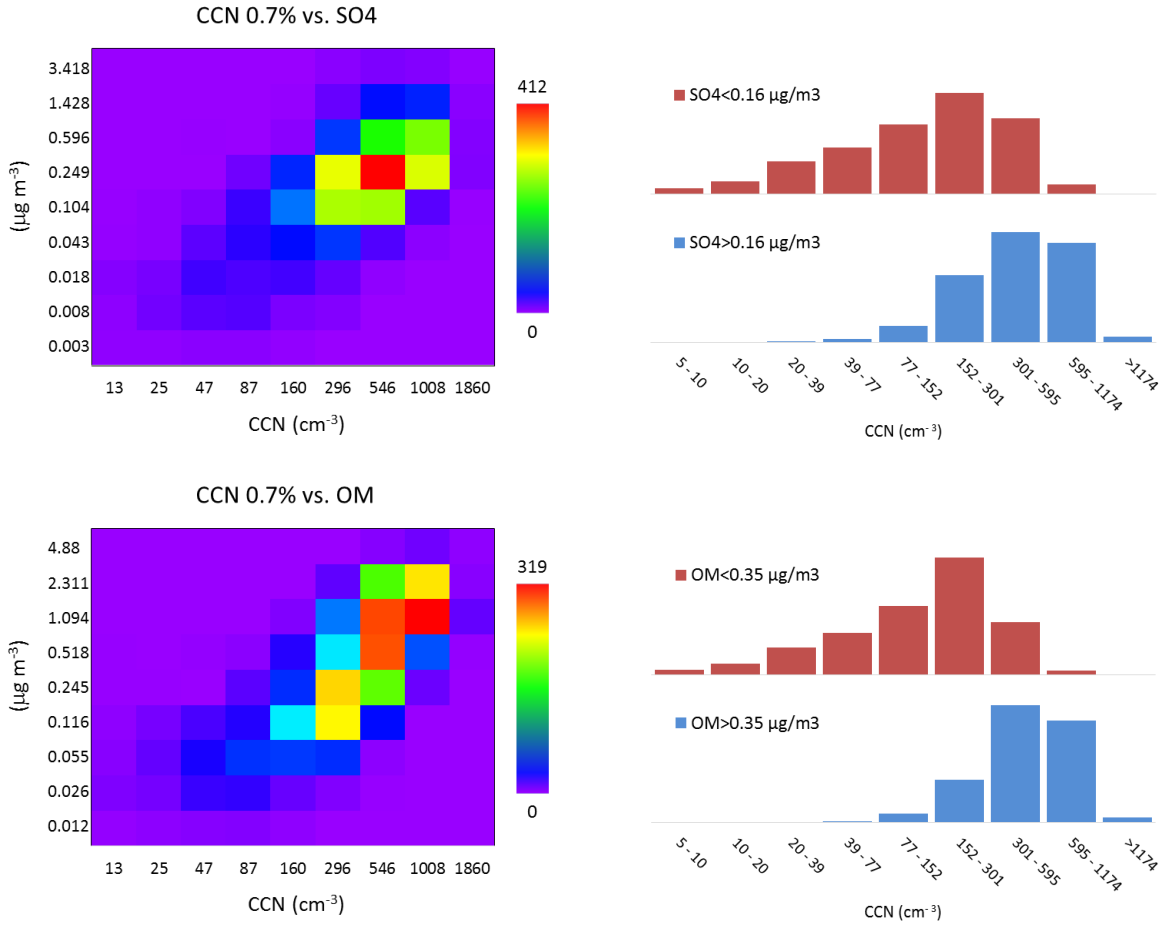

Figure 3.2. Examples of joint frequency distributions between CCN at 0.7% and SO_4 (top) or OM (bottom) for JFJ. The labels of the x and y axes represent the average concentrations (geometric mean) in each concentration bin. The colors indicate the number or hourly observations in each histogram column. The frequency distributions of CCN at given intervals of concentrations of SO_4 or OM are plotted in the right panels.

In general, the statistical correlation between CCN and ACSM species concentrations is expected to be higher for CCN at small *S* levels than at high *S*, because there is a greater overlap between the aerosol population carrying aerosol mass and the CCN at small *S* than at high *S* levels. This is clearly exemplified by the good correlation between aerosol SO_4 and CCN concentrations at 0.1% observed at Hyytiälä (SMR) which must compare with the poor correlation observed for CCN at 1% at the same station (Figure 3.5, top). However, the same dataset shows that the correlation between CCN and OM concentrations is larger for the high *S* regime than for the low *S* levels (Figure 3.5, bottom), indicating that the build-up of particulate OM is related to the formation of ultrafine CCN than of large CCN particles.

To summarize, the climatology of CCN concentrations observed concomitantly with aerosol chemical composition and visualized by joint frequency distributions shows a great diversity of behaviors, which reflect the complexity of atmospheric processes occurring at the specific sites.

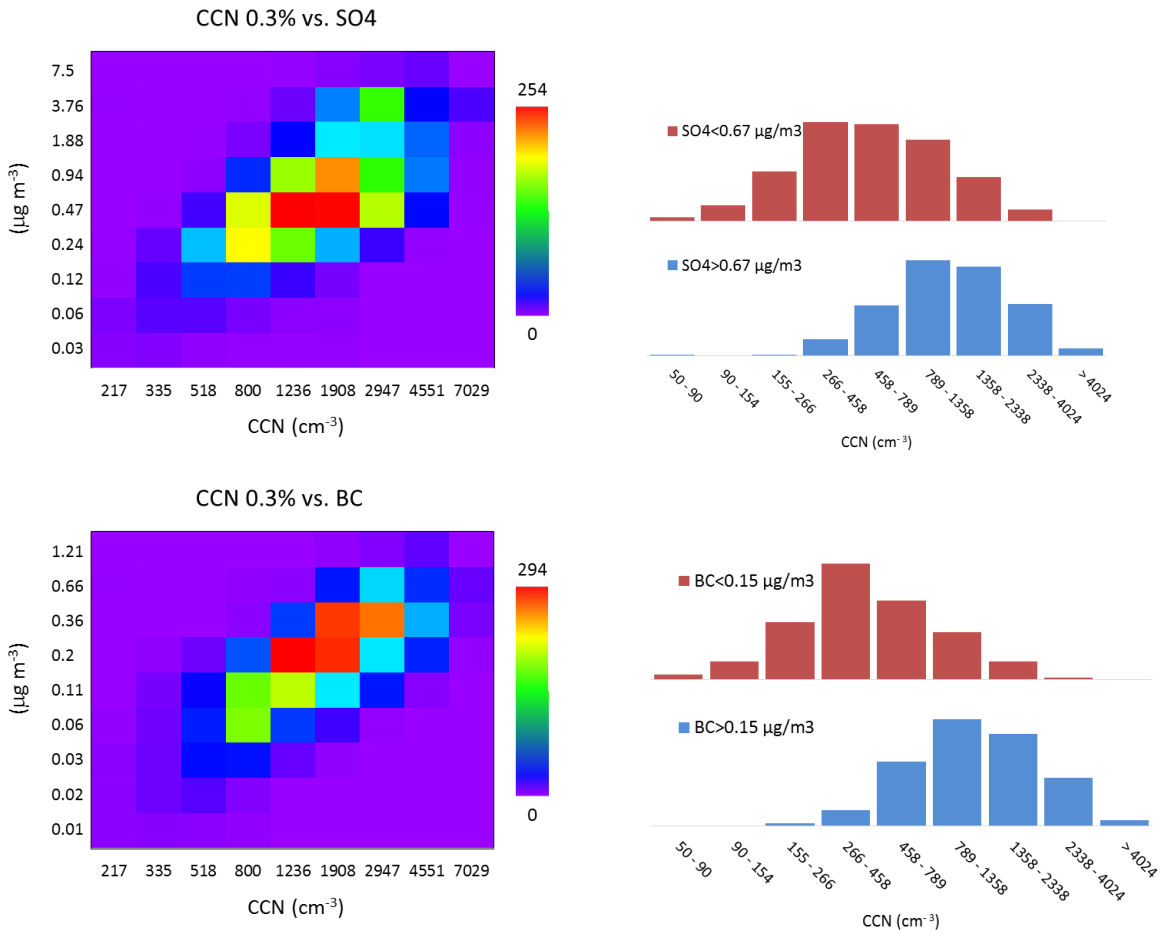

Figure 3.3. Examples of joint frequency distributions for CBW (left). The labels of the x and y axes represents the average concentrations (geometric mean) in each concentration bin. The colors indicate the number or hourly observations in each histogram column. The frequency distributions of CCN at given intervals of concentrations of SO_4 or BLACK CARBON are plotted in the right panels.

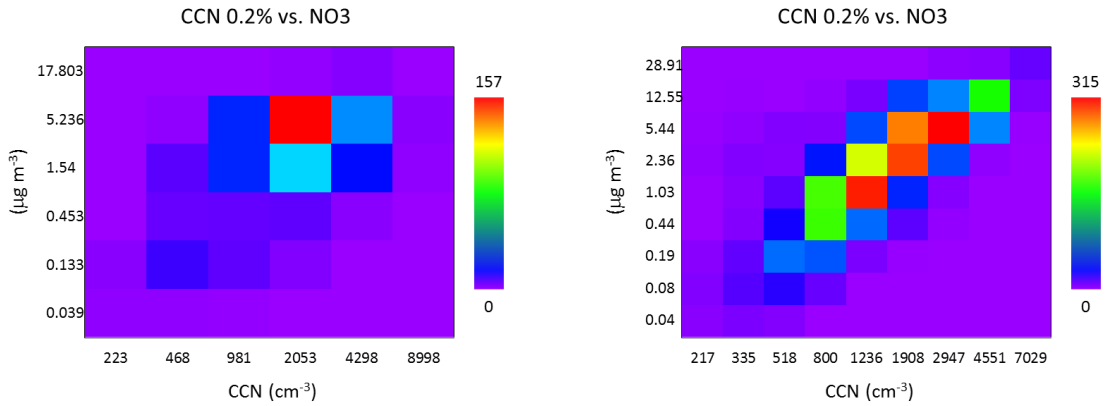

Figure 3.4. Examples of joint frequency distributions between NO_3 and CCN at 0.2% S for SPC (left) and CBW (right). (see the captions of Figure 3.2 or 3.3 for explanation of the axes).

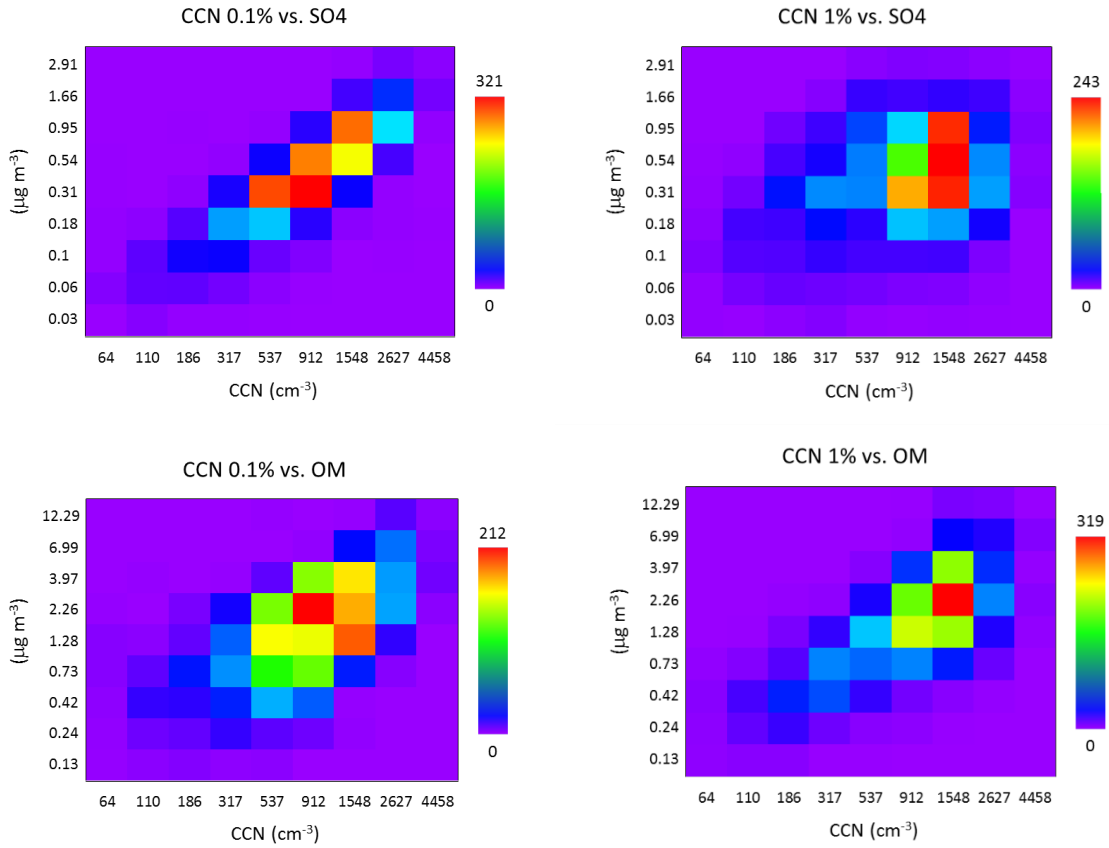

Figure 3.5. Examples of joint frequency distributions at Hyytiälä (SMR): for CCN at 0.1% S (left) and 1% S (right), and for SO_4 (top) and OM (bottom). (see the captions of Figure 3.2 or 3.3 for explanation of the axes).

The measure of intercorrelation between two discrete variables in a contingency table can be expressed through statistics such as the Cramér's V parameter. This is calculated using the following formula:

$$V = \sqrt{\frac{\chi^2/n}{\min(k-1, r-1)}}$$

where χ^2 is the chi-squared statistic, *n* is the total number of observations and *k* and *r* are the numbers of columns and rows. Cramér's V may be viewed as the association between two variables as a percentage of their maximum possible variation. It varies between 0 and +1.
Figure 3.6 reports the Cramér's V statistics (hereafter *V*) for the 128 contingency tables, classified per station, *S* of CCN, and per chemical parameter. Listed below some observations:

- In general, *V* values decrease with *S* (the chemistry of accumulation mode particles measured by the AMS becomes progressively less correlated with the concentrations of ultrafine particles of decreasing diameters). There are, however, several exceptions.
- The most remote station, JFJ, shows the least variability of *V* values, both between *S* ranges and between chemical variables. This can be explained by the fact that the aerosol at JFJ is prevalently transported to the site, with little local sources, and with aerosol chemical components relatively well internally-mixed.
- *V* values at MHD are also stable between *S* ranges, while Black Carbon concentration shows lower contingency with CCN concentrations when compared to non-refractory species. This might reflect the effect of sources of Black Carbon particles, which are not good CCN.
- In Hyytiälä (SMR), there is a great variability both between *S* ranges and between chemicals, reflecting the complexity of sources, state of mixing and aerosol size distribution at this site. The concentrations of sulfate aerosols show high contingency with those of CCN at 0.1% *S*, then *V* values drop at higher *S* and are insignificant at 1% *S*. In other words, the formation and accumulation of sulfate aerosols is correlated with the concentrations of CCN at 0.1% SS at the site, and is independent of the CCN at 1% *S*. This can be explained by considering CCN at 0.1% as mainly hygroscopic (sulfate-containing) accumulation mode particles and CCN at 1% as ultrafine particles whose formation involves other aerosol chemical components. The opposite trend of *V* for OM suggests that CCN at 1% are governed by the formation of organic particles. More precisely, the formation of organic mass occurred concomitantly to the increase of the concentrations of CCN at high SS. Since the positive trend of *V* for organics at increasing *S* ranges is not accompanied by a parallel increase of *V* for Black Carbon, we can hypothesize that the formation of organic compounds taking part in the build-up of CCN at 1% *S* is mainly a secondary process (new particle formation, NPF).
- The intercorrelation between CCN and aerosol chemical compound concentrations in MPZ is qualitatively similar to the SMR case: *V* values are high for sulfate at small *S* and drop at high *S* values, while *V* values for organics are initially small then increase at high *S*. In MPZ, the contingency between nitrate and CCN shows the same behavior of sulfate, while Black Carbon shows increasing *V* values at intermediate *S* values, indicating that the formation of carbonaceous particles including primary combustion particles plays a role in triggering the formation of CCN between 0.2 and 0.5% *S* at the site.
- In CBW, the degree of contingency between aerosol chemical parameters at CCN concentrations at small supersaturations (0.1%) is higher for inorganic secondary components (sulfate and nitrate) than for the carbonaceous species, indicating that CCN at 0.1% *S* are governed by hygroscopic accumulation mode particles at the site. At higher *S* ranges, the *V* values for sulfate aerosol drop like in SMR and MPZ, however the values for nitrate remains high, and stably higher than for all other three components. The reason why the formation of nitrate, which is normally found in large accumulation mode particles, is correlated with ultrafine CCN particles is unclear. It could be an effect of NOy chemistry, involving organic nitrates, or ultrafine particle formation in this environment.

- In the Po Valley, the best correlation between aerosol chemical components and CCN concentrations is found for carbonaceous aerosols, with the *V* values for Black Carbon approaching those for OM, hence pointing to primary combustion sources of CCN, which is expected as the campaign was carried out in winter at a rural site.

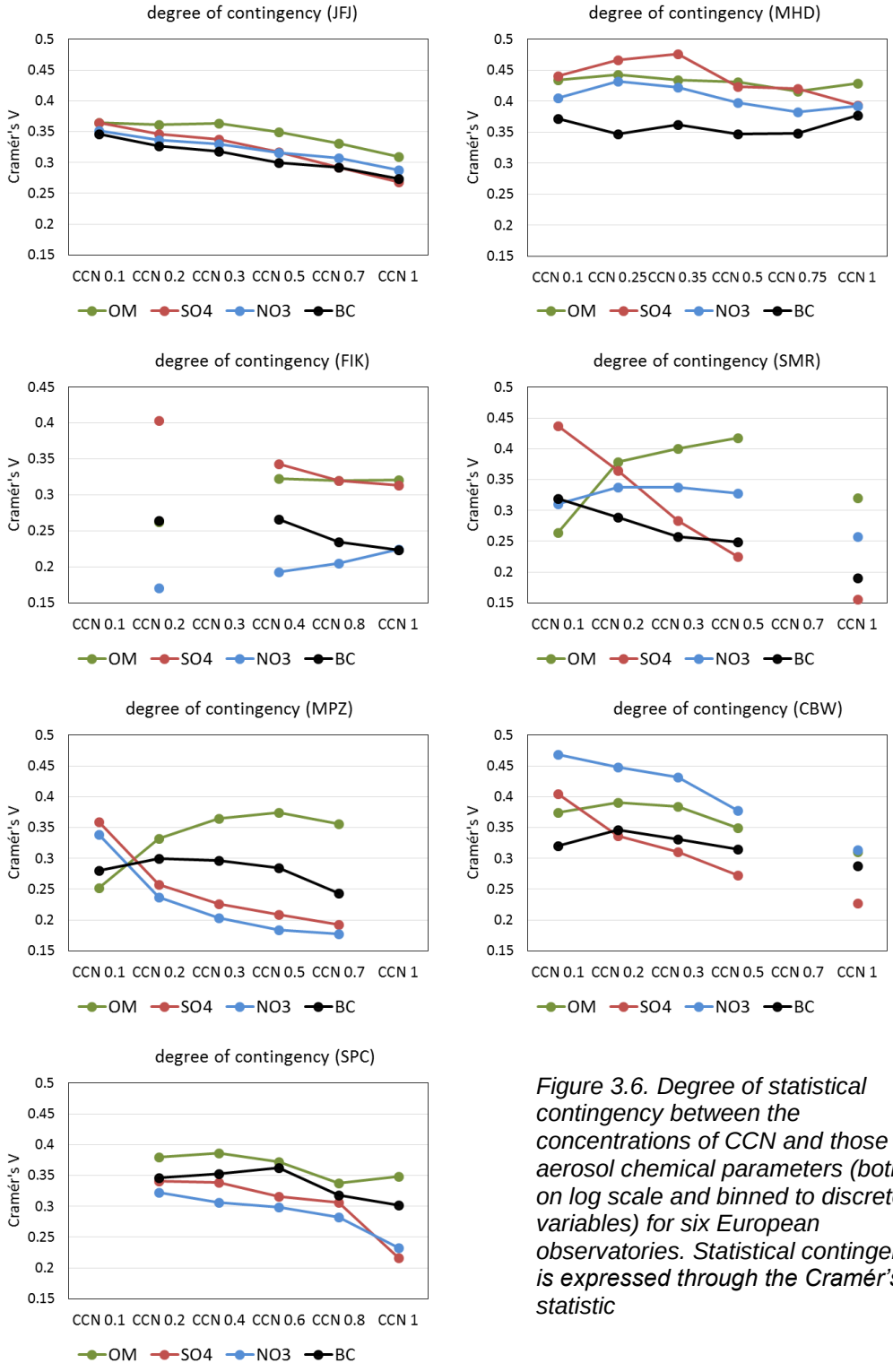

Figure 3.6. Degree of statistical contingency between the concentrations of CCN and those of aerosol chemical parameters (both on log scale and binned to discrete variables) for six European observatories. Statistical contingency is expressed through the Cramér's V statistic

4. Contribution from task 1.5 "Obtaining the vertical structure of aerosols and clouds" (TROPOS, HUJI, CUT, CNRS- GAME, and further BACCHUS and non-BACCHUS field campaign partners)

The goal of task 1.5 was to investigate aerosol-cloud interaction in the boundary layer (mostly liquid-water cloud layers) and in the free troposphere (here the focus is on mixed-phase cloud layers). These observations (case studies, general findings) can be used by the BACCHUS modelling groups. Satellite remote sensing efforts are presented in section 4.1, deals with boundary layer clouds and results from active remote sensing are presented in sections 4.2 and 4.3.

4.1 Progress in satellite remote sensing of aerosol-cloud interaction (HUJI)

The following excerpt is the abstract of a paper by Rosenfeld et al. (2016) in PNAS, titled "*Satellite retrieval of cloud condensation nuclei concentrations by using clouds as CCN chambers*":

"Quantifying the aerosol/cloud-mediated radiative effect at a global scale requires simultaneous satellite retrievals of cloud condensation nuclei (CCN) concentrations and cloud base updraft velocities (W_b). Hitherto, the inability to do so has been a major cause of high uncertainty regarding anthropogenic aerosol/cloud-mediated radiative forcing. This can be addressed by the emerging capability of estimating CCN and W_b of boundary layer convective clouds from an operational polar orbiting weather satellite. Our methodology uses such clouds as an effective analog for CCN chambers. The cloud base supersaturation (S) is determined by W_b and the satellite-retrieved cloud base drop concentrations (N_{db}), which is the same as CCN(S). Validation against ground-based CCN instruments at Oklahoma, at Manaus, and onboard a ship in the northeast Pacific showed a retrieval accuracy of ±25% to ±30% for individual satellite overpasses. The methodology is presently limited to boundary layer not raining convective clouds of at least 1 km depth that are not obscured by upper layer clouds, including semitransparent cirrus. The limitation for small solar backscattering angles of <25° restricts the satellite coverage to ~25% of the world area in a single day."

The commonly used CCN counters measure the number concentration of aerosol particles in a sample air stream (N_a), which at a given S can be activated into the same number of cloud droplets at its base (N_{db}). Alternatively, retrieving N_{db} and S in clouds can provide CCN(S). The peak vapor supersaturation at an adiabatic cloud base, S, is determined by CCN(S) and W_b. Therefore, a good approximation of S can be calculated from the retrieved N_{db} and W_b according to

$$S=C(T_b, p_b)\, W_b^{3/4} N_{db}^{-1/2} \quad (1)$$

where C is a coefficient that depends weakly on cloud base temperature (T_b) and pressure (p_b) (Pinsky et al., 2012). This is an analytical expression that was derived based on theoretical considerations. Recently, it has become possible to estimate N_{db} and W_b from satellite measurements, thus calculating also S. This constitutes the ability to calculate CCN(S) from satellite measurements only.

We have developed the ability to retrieve from satellites both N_{db} (Freud et al., 2011; Rosenfeld et al., 2014) and W_b (Zhu et al., 2014) for convective clouds, and validated it over the ASR sites in the Southern Great Plains, during the GO-Amazon campaign, and over the MAGIC ship campaign at the northeast Pacific Ocean.

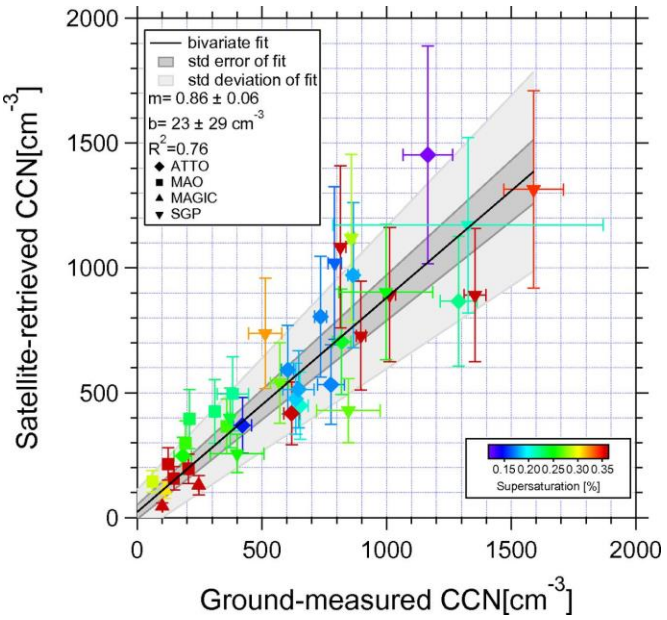

Figure 4.1: The relationship between satellite-retrieved CCN concentration and S at cloud base, and the ground-based instrument measurements of CCN concentration at the same S. The slope and intercept of the best fit line are given in the key by m and b, respectively. The validation data are collected from the DOE/ASR sites on the SGP in Oklahoma and GOAmazon near Manaus, and over the northeast Pacific (MAGIC). In addition, data are obtained from the ATTO. The location is denoted by the marker shape, and S is shown by the color. Figure taken from Rosenfeld et al. (2016).

The retrieved N_{db} is validated against ground based measured CCN at the satellite retrieved S, as shown in Figure 4.1. The validation error includes the combined errors of the retrieval of W_b, N_{db}, S, and the ground based errors of CCN measurements. The standard error of estimate is near ±30%. This renders satellite retrievals as a useful practical tool for mapping at a global scale the CCN and S at which the aerosols are actually activated into droplets at the base of the convective clouds.

We have been extending the validation to CCN measurements from the BACCHUS campaign. An ideal validation site, such as the ASR sites used in Figure 4.1, has validation of cloud base height and updraft by Doppler lidar or radar, in addition to the validation of the CCN(S).

4.1.1 Inaccurate radiosonde estimates of cloud base height and temperature

We recently encountered several issues with the estimates of cloud base height from radiosondes. Radiosonde data does not represent sufficiently accurate cloud base temperature (T_b) and height. This was found by comparing ceilometer to radiosonde cloud base temperatures, as shown in Figure 4.2. The figure shows that radiosonde estimates of T_b can have large deviations from the actually measured T_b as inferred by the ceilometer measured cloud base height and a dry adiabatic lapse rate from the ground to that height. The satellite retrieved T_b is in much better agreement with the ceilometer-based T_b. The estimates based on reanalysis data were even worse than the radiosondes.

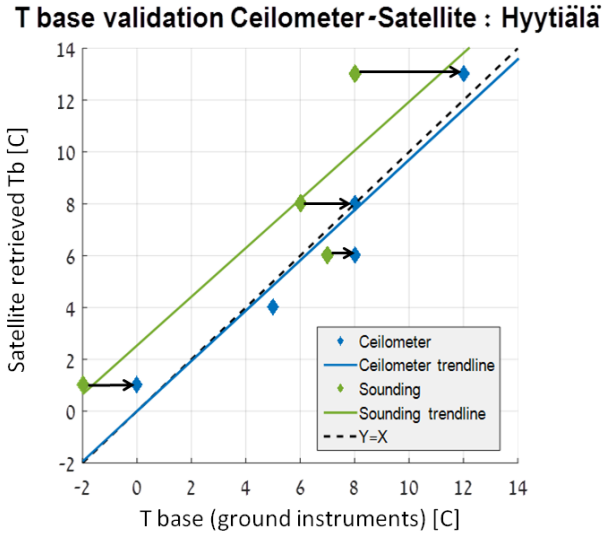

Figure 4.2: Validation of satellite-retrieved cloud base temperature against ceilometer and radiosonde in Hyytiälä.

4.1.2 Loss of sensitivity at cold and clean cloud base

Cloud base is determined by its visible reflectance exceeding a given threshold. However, clouds with colder base have less water for a given cloud geometrical depth above base. Clouds developing in cleaner air have smaller number concentration of larger drops. Both effects render the clouds being less reflective for solar radiation, and thus cloud bases can go undetected resulting in underestimation of T_b. To remedy this problem we developed a correction algorithm, which uses the SBDART radiative transfer model to calculate cloud base reflectance based on the retrieved N_{db} and T_b. This reflectance is used as a new threshold for calculating a new set of N_{db} and T_b, which is in turn used to calculate a new cloud base reflectance. This is repeated in iterations until the solution converges. A validation site where this played a significant role is Mace Head, shown in Figure 4.3. The correction in T_b was essential for obtaining correct CCN.

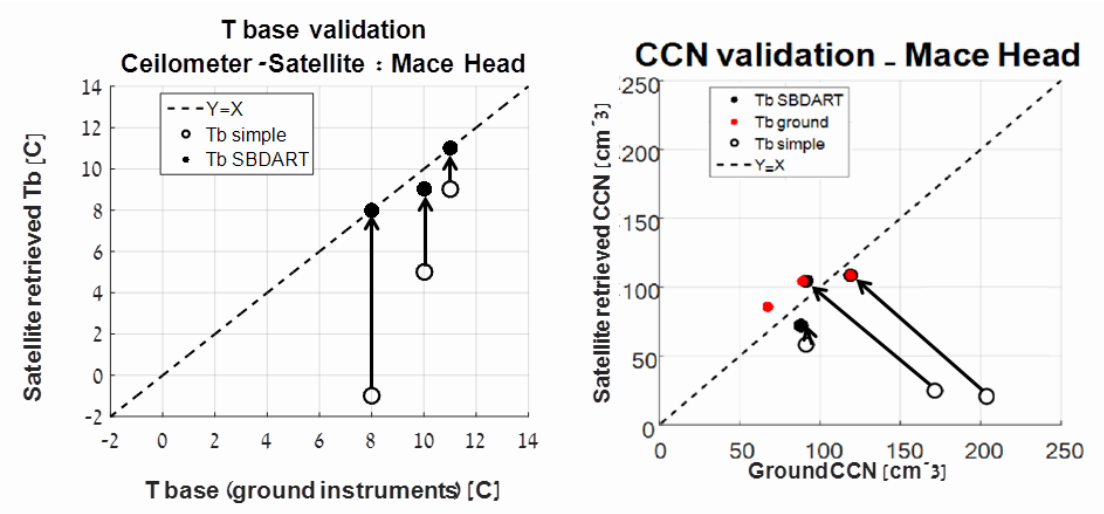

Figure 4.3. Left panel: Validation of satellite-retrieved cloud base temperature at Mace Head using ceilometer, before (T_b simple) and after (T_b SBDART) the iterative correction with SBDART. Right panel: the impact of the correction of T_b on the retrieved CCN.

4.1.3 Need to improve cloud base updrafts under low solar declination

We have observed a systematic underestimate of CCN in high latitudes, especially in winter during low solar declination. It is suspected that the weaker solar heating over land produces weaker updrafts, which then produce smaller S than inferred by the present algorithm, which, in such case, overestimates W_b. This causes an overestimation of S, which matches to respectively larger CCN at the ground measurements. From the satellite retrieval point of view this is an underestimation of the CCN. This is evident in Figure 4.4, which shows satellite underestimate of CCN especially for Hyytiala and winter Cabauw. A tropical site (Manacapuru near Manaus) showed no such bias. Figure 4.4 shows also that there is room for improving the accuracy of retrieving CCN by improving the accuracy of retrieved T_b, especially at northern latitudes.

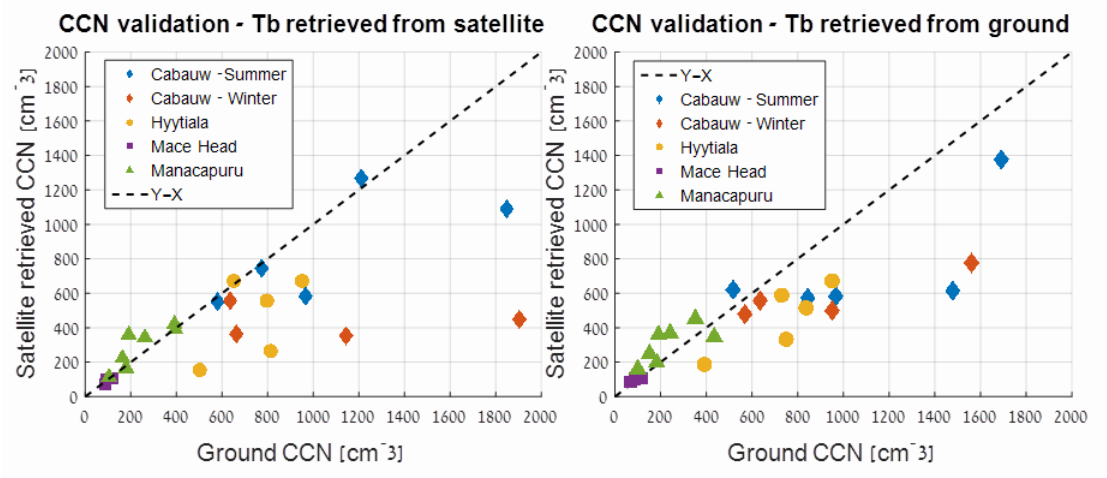

Figure 4.4. Validation of satellite retrieved CCN for several sites. Underestimation is evident mostly for sites of low solar declination.

4.1.4 Next steps

Additional validation efforts are being performed also on Finokalia (Crete), Cyprus, COPE data sets, and additional data from the already analyzed sites. Work for improving the accuracy is under way. Finally, application to initial satellite maps of CCN over large areas is also under way, and will be reported next time.

4.2 Active remote sensing of mixed-phase clouds with Cloudnet

4.2.1 Cloudnet studies

The remote sensing group of TROPOS has concentrated on evaluation of data sets from different Cloudnet stations. Universal methods have been developed to analyze ice formation within mixed-phase cloud layers throughout the different Cloudnet datasets. For example, a new method has been developed to measure the rate of ice formation in mixed-phase cloud layers (Bühl et al., 2016). Ice water content (*IWC*) is measured at a distance of 60 m below the base of mixed-phase cloud layers with a cloud radar and by means of the method of Hogan et al. (2006). The distance between the mixed-phase layer and the measurement volume allows undisturbed characterization of ice crystals with no interfering cloud radar signals from turbulent cloud top. Also, particle evaporation, aggregation or other processes altering number or shape of particles have not yet

taken place. The method allows characterization of *IWC* and particle fall velocity *v* (see Fig. 4.5) for derivation of a simple representation of ice mass flux *F* = *IWC* x *v* from the mixed-phase cloud top layer (see Fig. 4.6). *F* is directly proportional to the rate of ice formation in the mixed-phase cloud and allows characterization of ice formation efficiency under different regimes of temperature and/or particles shape. Furthermore, measurements of liquid water path (*LWP*) and *F* allow estimating a static cloud lifetime index (Fig. 4.6b) by simply dividing *LWP* and *F*. The resulting time indicates how long it would need for the ice formation to completely consume all liquid water present within the cloud layer, assuming no vertical motion. In this way, the impact of ice formation on clouds has been measured directly and compared for different temperature regimes.

The method of Bühl et al. (2016), presented here, is automated and by design applicable to any Cloudnet dataset. So far, the method has been used to analyze properties of mixed-phase cloud layers at Mace Head, Leipzig, Lindenberg, Potenza, Chilbolton and Barbados Cloudnet datasets. Figure 4.7 shows the measurements of *F* for all Cloudnet observation stations and indicates that - surprisingly - the differences in ice formation efficiency is quite low between the different stations. In future, this new evaluation method will be the starting point in order to compare the existing datasets of ice formation, e.g., with aerosol statistics derived from Raman lidar observations at Leipzig, to systematically search for links between given aerosol conditions and cloud properties. The Leipzig Cloudnet station was recently moved to Limassol, Cyprus, for one year, to measure aerosol and cloud layers in a region dominated by complex aerosol layering of desert dust, biomass burning smoke, and anthropogenic haze. Middle East climate conditions are prevailing in the Cyprus region.

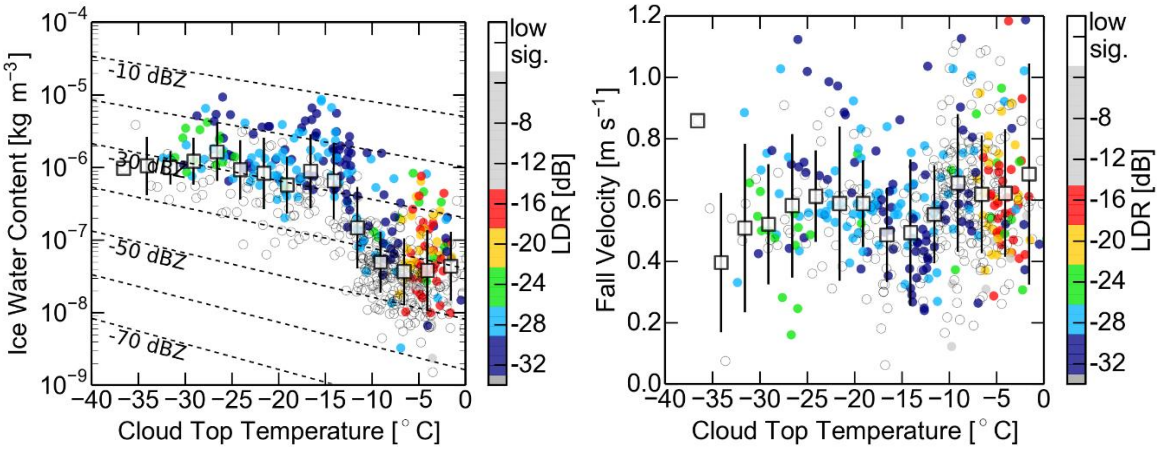

Figure 4.5. (a) Left: Ice water content (IWC) 60m below the basis of the mixed-phase cloud layers. Detection thresholds for different radar sensitivities are indicated as dashed lines. Colors indicate corresponding particles Linear Depolarization Ratio (LDR). (b) Right: Corresponding fall velocity of particles as detected by cloud radar.

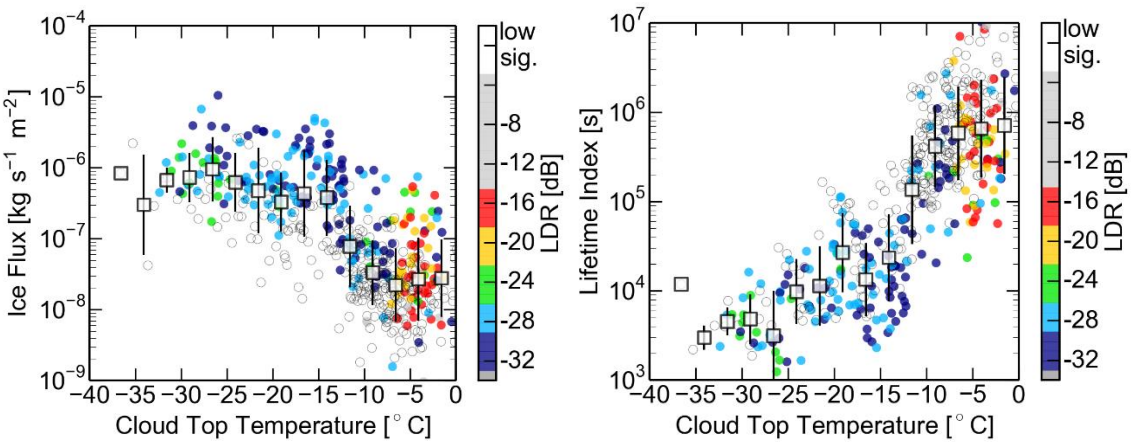

Figure 4.6. (a) Left: Mass flux of ice *F* = *IWC* x *v* (see Fig. 1). (b) Right: Liquid water path divided by *F* resulting in an estimation of cloud lifetime assuming static conditions.

4.2.2 CCN and INP profiles estimated from polarization lidar

We developed a new method to estimate CCN concentration profiles and INP number concentration profiles from polarization lidar observations (Mamouri and Ansmann, 2016). We applied this method to estimate INP profiles just before ice-containing cloud layers crossed the lidar site. The INP profile values (at cloud level) were then compared with the number concentration of ice crystals, produced in the layered cloud and falling out of the altocumulus. The crystal fall speed and thus the size and of the particles was observed with Doppler lidar. The size of the falling ice crystals together with cloud parcel extinction coefficient yield an estimate of the ice crystal (IC) number concentration. Good agreement was found between the estimated INP number concentration at cloud level and IC number concentration, as long as the temperatures were around -30°C or higher. At lower temperatures, homogeneous freezing dominates and closure between INP and IC number concentrations is no longer obtained. The closure study was presented at EGU, Vienna, in spring 2016. Further closure studies are currently performed based on the Cyprus 2015 campaign data and will be completed in 2017.

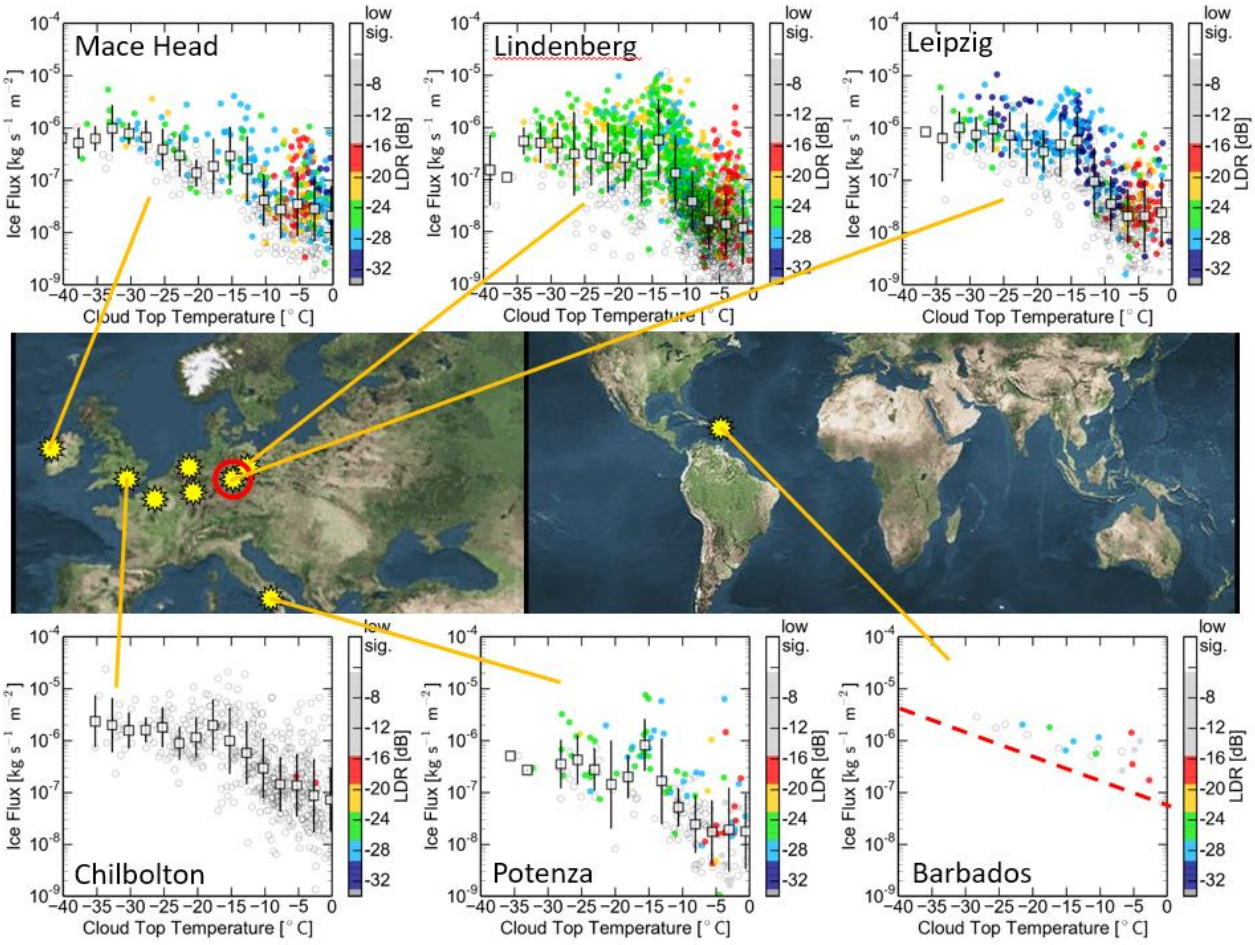

Figure 4.7. Measurements of ice mass flux (F, see Fig. 4.2) measured for different Cloudnet stations. For Barbados station, current estimation of instrument sensitivity is indicated as a dashed line.

Changes with respect to the DoW

No major deviation from the DoW have occurred.

Dissemination and uptake

The results of the Deliverable 1.3 have been disseminated outside the BACCHUS community by presentations at the National and international Conferences and Workshops

Main results have also been disseminated through published articles.

Peer-reviewed publications:

- Bianchi, F., Tröstl, J., Junninen, H., Frege, C., Henne, S., Hoyle, C. R., Molteni, U., Herrmann, E., Adamov, A., Bukowiecki, N., Chen, X., Juplissy, J., Gysel, M, Hutterli, M. Kangasluoma, J., Kontkanen, J., Kürten, A., Manninen, H. E., Münch, S., Peräkylä, O., Petäjä, T., Rondo, L., Williamson, C., Weingartner, E., Curtius, J., Worsnop, D. R. , M. Kulmala, M., Dommen, J., Baltensperger, U.: New particle formation in the free troposphere: A question of chemistry and timing. Science, doi: 10.1126/science.aad5456, 2016.

- Boose et al. 2016b, Ice Nucleating Particle Measurements at 241 K during Winter Months at 3580 m MSL in the Swiss Alps. J. Atmos. Sci., 73, doi:10.1175/JAS-D-15-0236.1, 2016.

- Herrmann, E., Weingartner, E., Henne, S., Vuilleumier, L., Bukowiecki, N., Steinbacher, M., Conen, F., Collaud Coen, M., Hammer, E., Juranyi, Z., Baltensperger, U., and Gysel, M.: Analysis of long-term aerosol size distribution data from Jungfraujoch with emphasis on free tropospheric conditions, cloud influence, and air mass transport, J. Geophys. Res. Atmos., 120, doi:10.1002/2015JD023660, 2015.

- Kirillova, E. N., A. Marinoni, P. Bonasoni, E. Vuillermoz, M. C. Facchini, S. Fuzzi, and S. Decesari: Light absorption properties of brown carbon in the high Himalayas, J. Geophys. Res. Atmos., 121, doi:10.1002/2016JD025030, 2016.

- Kirkby, J. et al.: Ion-induced nucleation of pure biogenic particles, Nature, 533, doi:10.1038/nature17953, 2016.

- Rosenfeld D., Y. Zheng, E. Hashimshoni, M. L. Pöhlker, A. Jefferson, C. Pöhlker, X. Yu, Y. Zhu, G. Liu, Z. Yue, B. Fischman, Z. Li, D. Giguzin, T. Goren, P. Artaxoi, H. M. J. Barbosai, U. Pöschl, and Meinrat O. Andreae: Satellite retrieval of cloud condensation nuclei concentrations by using clouds as CCN chambers. Proceedings of the National Academy of Sciences, doi:10.1073/pnas.1514044113, 2016.

- Stopelli, E., Conen, F., Morris, C. E., Herrmann, E., Bukowiecki, N., and Alewell, C.: Ice nucleation active particles are efficiently removed by precipitating clouds, Sci. Rep., 5, doi: 10.1038/srep16433, 2015.

- Tröstl, J. et al.: The role of low-volatility organic compounds in initial particle growth in the atmosphere, Nature, 533, doi: 10.1038/nature1827, 2016.

- Tröstl, J. et al.: Contribution of new particle formation to the total aerosol concentration at the high-altitude site Jungfraujoch (3580 m asl, Switzerland), J. Geophys. Res. Atmos., 121, doi: 10.1002/2015JD024637, 2016.

- Vergara Temprado, J., Wilson, T. W., O'Sullivan, D., Browse, J., Pringle, K. J., Ardon-Dryer, K., Bertram, A. K., Burrows, S. M., Ceburnis, D., DeMott, P. J., Mason, R. H., O'Dowd, C. D., Rinaldi, M., Murray, B. J., and Carslaw, K. S.: Contribution of feldspar and marine organic aerosols to global ice nucleating particle concentrations, Atmos. Chem. Phys. Discuss., doi:10.5194/acp-2016-822, in review, 2016.

- Wilson T. W. et al.: A marine biogenic source of atmospheric ice-nucleating particles, Nature, 525, doi: 10.1038/nature14986, 2016.

- Xu, C., Hantson, S., Holmgren, M., van Nes, E. H., Staal, A., and Scheffer, M.: Remotely sensed canopy height reveals three pantropical ecosystem states, Ecology, 97(9), 2016.

- Zhu Y, et al.: Satellite retrieval of convective cloud base temperature based on the NPP/VIIRS Imager. Geophys Res Lett 41(4):1308–1313, 2014.

Open Access Journal (as "Atmospheric Chemistry and Physics Discussion)

- Boose, Y., Sierau, B., García, M. I., Rodríguez, S., Alastuey, A., Linke, C., Schnaiter, M., Kupiszewski, P., Kanji, Z. A., and Lohmann, U.: Ice nucleating particles in the Saharan Air Layer, Atmos. Chem. Phys., 16, 9067-9087, doi:10.5194/acp-16-9067-2016, 2016.

- Bühl, J., Seifert, P., Myagkov, A., and Ansmann, A.: Measuring ice- and liquid-water properties in mixed-phase cloud layers at the Leipzig Cloudnet station, Atmos. Chem. Phys., 16, 10609-10620, doi:10.5194/acp-16-10609-2016, 2016.

- Crawford, I., Lloyd, G., Herrmann, E., Hoyle, C. R., Bower, K. N., Connolly, P. J., Flynn, M. J., Kaye, P. H., Choularton, T. W., Gallagher, M. W.: Observations of fluorescent aerosol–cloud interactions in the free troposphere at the High-Altitude Research Station Jungfraujoch, Atmos. Chem. Phys., 16, 2273–2284, doi: 10.5194/acp-16-2273-2016, 2016.

- Hammer, E., Bukowiecki, N., Luo, B. P., Lohmann, U., Marcolli, C., Weingartner, E. Baltensperger, U., and Hoyle, C. R.: Sensitivity estimations for cloud droplet formation in the vicinity of the high-alpine research station Jungfraujoch (3580ma.s.l.), Atmos. Chem. Phys., 15, 10309–10323, doi: 10.5194/acp-15-10309-2015, 2015.

- Hoyle, C.R. Webster, C. S., Rieder, H. E., Nenes, A., Hammer, E., Herrmann, E., Gysel, M, Bukowiecki, N. Weingartner, E., Steinbacher, M. and Baltensperger, U.: Chemical and physical influences on aerosol activation in liquid clouds: a study based on observations from the Jungfraujoch, Switzerland, Atmos. Chem. Phys., 16, 4043–4061, doi: 10.5194/acp-16-4043-2016, 2016.

- Hoyle, C. R. et al.: Aqueous phase oxidation of sulphur dioxide by ozone in cloud droplets, Atmos. Chem. Phys., 16, 1693–1712, doi:10.5194/acp-16-1693-2016, 2016.

- Kalivitis, N., Kerminen, V.-M., Kouvarakis, G., Stavroulas, I., Bougiatioti, A., Nenes, A., Manninen, H. E., Petäjä, T., Kulmala, M., Mihalopoulos, N.: Atmospheric new particle formation as a source of CCN in the eastern Mediterranean marine boundary layer, Atmos. Chem. Phys., 15, 9203–9215, doi:10.5194/acp-15-9203-2015, 2015.

- Mamouri, R.-E. and Ansmann, A. (2016) Potential of polarization lidar to provide profiles of CCN- and INP-relevant aerosol parameters, Atmos. Chem. Phys., 16, 5905-5931, doi:10.5194/acp-16-5905-2016, 2016.

- O'Dowd, C.D., D. Ceburnis, J. Ovadnevaite, J. Bialek, D. B. Stengel, M. Zacharias, U. Nitschke, S. Connan, M. Rinaldi, S. Fuzzi, S. Decesari, M. C. Facchini, S. Marullo, R. Santoleri, A. Dell'Anno, C. Corinaldesi, M. Tangherlini and R. Danovaro: Connecting marine productivity to sea-spray via nanoscale biological proceses: Phytoplankton Dance or Death Disco? Scientific Reports, Volume 5, Article number 14883, 2015.

- Pöhlker, M. L., Pöhlker, C., Klimach, T., Hrabe de Angelis, I., Barbosa, H. M. J., Brito, J., Carbone, S., Cheng, Y., Chi, X., Ditas, F., Ditz, R., Gunthe, S. S., Kesselmeier, J., Könemann, T., Lavrič, J. V., Martin, S. T., Moran-Zuloaga, D., Rose, D., Saturno, J., Su, H., Thalman, R., Walter, D., Wang, J., Wolff, S., Artaxo, P., Andreae, M. O., and Pöschl, U.: Long-term observations of atmospheric aerosol, cloud condensation nuclei concentration and hygroscopicity in the Amazon rain forest – Part 1: Size-resolved characterization and new model parameterizations for CCN prediction, Atmos. Chem. Phys., accepted, 2016.

- Rinaldi, M., Gilardoni, S., Paglione, M., Sandrini, S., Fuzzi, S., Massoli, P., Bonasoni, P., Cristofanelli, P., Marinoni, A., Poluzzi, V., and Decesari, S.: Organic aerosol evolution and transport observed at Mt. Cimone (2165 m a.s.l.), Italy, during the PEGASOS campaign, Atmos. Chem. Phys., 15, doi:10.5194/acp-15-11327-2015, 2015.

- Rosati, B., M. Gysel, F. Rubach, T. F. Mentel, B. Goger, L. Poulain, P. Schlag, P. Miettinen, A. Pajunoja, A. Virtanen, J. Bialek, H. Klein Baltink, J. S. Henzing, J. Größ, G. P. Gobbi, A. Wiedensohler, A. Kiendler-Scharr, C. O'Dowd, S. Decesari, M. C. Facchini, E. Weingartner, and U. Baltensperger, Vertical profiling of aerosol hygroscopic properties in the planetary boundary layer during the PEGASOS campaigns . Atmos. Chem. Phys., 16, 7295-7315, 2016.

- Sandrini, S., van Pinxteren, D., Giulianelli, L., Herrmann, H., Poulain, L., Facchini, M. C., Gilardoni, S., Rinaldi, M., Paglione, M., Turpin, B. J., Pollini, F., Bucci, S., Zanca, N., and Decesari, S.: Size-resolved aerosol composition at an urban and a rural site in the Po Valley in summertime: implications for secondary aerosol formation, Atmos. Chem. Phys., 16, doi:10.5194/acp-16-10879-2016, 2016.

- Schrod, J., Danielczok, A., Weber, D., Ebert, M., Thomson, E. S., and Bingemer, H. G.: Re-evaluating the Frankfurt isothermal static diffusion chamber for ice nucleation, Atmos. Meas. Tech., 9, 1313-1324, doi:10.5194/amt-9-1313-2016, 2016.

- Stopelli E., Conen, F., Morris, C. E., Herrmann, E., Henne, S. Steinbacher, M. and Alewell, C.: Predicting abundance and variability of ice nucleating particles in precipitation at the high-altitude observatory Jungfraujoch, Atmos. Chem. Phys., 16, 8341–8351, doi:10.5194/acp-16-8341-2016, 2016.

- Su, H., Cheng, Y., Ma, N., Wang, Z., Wang, X., Pöhlker, M. L., Nillius, B., Wiedensohler, A., and Pöschl, U.: A broad supersaturation scanning (BS2) approach for rapid measurement of aerosol particle hygroscopicity and cloud condensation nuclei activity, Atmos. Meas. Tech., 9, 5183-5192, doi:10.5194/amt-9-5183-2016, 2016.

- Yu, X., Wang, Z., Zhang, M., Kuhn, U., Xie, Z., Cheng, Y., Pöschl, U., and Su, H.: Ambient measurement of fluorescent aerosol particles with a WIBS in the Yangtze River Delta of China: potential impacts of combustion-related aerosol particles, Atmos. Chem. Phys., 16, 11337-11348, doi:10.5194/acp-16-11337-2016, 2016.

- Zieger, P., Aalto, P. P., Aaltonen, V., Äijälä, M., Backman, J., Hong, J., Komppula, M., Krejci, R., Laborde, M., Lampilahti, J., de Leeuw, G., Pfüller, A., Rosati, B., Tesche, M., Tunved, P., Väänänen, R., and Petäjä, T.: Low hygroscopic scattering enhancement of boreal aerosol and the implications for a columnar optical closure study, Atmos. Chem. Phys., 15, 7247–7267, doi:10.5194/acp-15-7247-2015, 2015.

References

- Boose, Y., Sierau, B., García, M. I., Rodríguez, S., Alastuey, A., Linke, C., Schnaiter, M., Kupiszewski, P., Kanji, Z. A., and Lohmann, U.: Ice nucleating particles in the Saharan Air Layer, Atmos. Chem. Phys., 16, 9067-9087, doi:10.5194/acp-16-9067-2016, 2016.
- Boose et al. 2016b, Ice Nucleating Particle Measurements at 241 K during Winter Months at 3580 m MSL in the Swiss Alps. J. Atmos. Sci., 73, doi:10.1175/JAS-D-15-0236.1, 2016.
- Bühl, J., Seifert, P., Myagkov, A., and Ansmann, A.: Measuring ice- and liquid-water properties in mixed-phase cloud layers at the Leipzig Cloudnet station, Atmos. Chem. Phys., 16, 10609-10620, doi:10.5194/acp-16-10609-2016, 2016.
- Carslaw et al. (2013) Nature 503, 67-71.
- Carslaw et al. (2016) Aerosol in the pre-industrial atmosphere, Submitted to Current Climate Change Reports 2016.
- Freud E, Rosenfeld D, Kulkarni J (2011) Resolving both entrainment-mixing and number of activated CCN in deep convective clouds. Atmos. Chem. Phys. 11(24):12887–12900.
- Douglas S. Hamilton, Lindsay A. Lee, Kirsty J. Pringle, Carly L. Reddington, Dominick V. Spracklen, and Kenneth S. Carslaw Occurrence of pristine aerosol environments on a polluted planet, PNAS 2014 111 (52) 18466-18471; published ahead of print December 15, 2014,doi:10.1073/pnas.1415440111Hiranuma, N., and Coauthors (2015) A comprehensive laboratory study on the immersion freezing behavior of illite NX particles: a comparison of 17 ice nucleation measurement techniques. Atmos. Chem. and Phys., 15, 2489–2518, doi:10.5194/acp-15-2489-2015.
- Hogan, R. J., Mittermaier, M. P., and Illingworth, A. J.(2006) The retrieval of ice water content from radar reflectivity factor and temperature and its use in evaluating a mesoscale model, J. Appl. Meteorol. Clim., 45, 301–317, doi:10.1175/JAM2340.1.
- Mamouri, R.-E. and Ansmann, A. (2016) Potential of polarization lidar to provide profiles of CCN- and INP-relevant aerosol parameters, Atmos. Chem. Phys., 16, 5905-5931, doi:10.5194/acp-16-5905-2016, 201
- Paramonov, M., Kerminen, V.-M., Gysel, M., Aalto, P. P., Andreae, M. O., Asmi, E., Baltensperger, U., Bougiatioti, A., Brus, D., Frank, G. P., Good, N., Gunthe, S. S., Hao, L., Irwin, M., Jaatinen, A., Jurányi, Z., King, S. M., Kortelainen, A., Kristensson, A., Lihavainen, H., Kulmala, M., Lohmann, U., Martin, S. T., McFiggans, G., Mihalopoulos, N., Nenes, A., O'Dowd, C. D., Ovadnevaite, J., Petäjä, T., Pöschl, U., Roberts, G. C., Rose, D., Svenningsson, B., Swietlicki, E., Weingartner, E., Whitehead, J., Wiedensohler, A., Wittbom, C., and Sierau, B.: A synthesis of cloud condensation nuclei counter (CCNC) measurements within the EUCAARI network, Atmos. Chem. Phys., 15, 12211-12229, doi:10.5194/acp-15-12211-2015, 2015.
- Pinsky M, Khain A, Mazin I, Korolev A (2012) Analytical estimation of droplet concentration at cloud base. J Geophys Res 117(D18):D18211.
- Pöhlker, M. L., Pöhlker, C., Klimach, T., Hrabe de Angelis, I., Barbosa, H. M. J., Brito, J., Carbone, S., Cheng, Y., Chi, X., Ditas, F., Ditz, R., Gunthe, S. S., Kesselmeier, J., Könemann, T., Lavrič, J. V., Martin, S. T., Moran-Zuloaga, D., Rose, D., Saturno, J., Su, H., Thalman, R., Walter, D., Wang, J., Wolff, S., Artaxo, P., Andreae, M. O., and Pöschl, U.: Long-term observations of atmospheric aerosol, cloud condensation nuclei concentration and hygroscopicity in the Amazon rain forest – Part 1: Size-resolved characterization and new model parameterizations for CCN prediction, Atmos. Chem. Phys., accepted, 2016.
- Riipinen et al., 2011

- Rinaldi, M., and Coauthors (2009) On the representativeness of coastal aerosol studies to open ocean studies: Mace Head–a case study. Atmos. Chem. and Phys., 9, 9635–9646.
- Rosenfeld D, Fischman B, Zheng Y, Goren T, Giguzin D (2014) Combined satellite and radar retrievals of drop concentration and CCN at convective cloud base. Geophys Res Lett 41(9):3259–3265.
- Rosenfeld D., Y. Zheng, E. Hashimshoni, M. L. Pöhlker, A. Jefferson, C. Pöhlker, X. Yu, Y. Zhu, G. Liu, Z. Yue, B. Fischman, Z. Li, D. Giguzin, T. Goren, P. Artaxoi, H. M. J. Barbosai, U. Pöschl, and Meinrat O. Andreae, (2016) Satellite retrieval of cloud condensation nuclei concentrations by using clouds as CCN chambers. Proceedings of the National Academy of Sciences, doi:10.1073/pnas.1514044113.
- Santachiara, G., Di Matteo, L., Prodi, F., Belosi, F., (2010) Atmospheric particles acting as Ice Forming Nuclei in different size ranges, Atmos. Res. 96, 266-272.
- Schmale et al., Collocated observations of cloud condensation nuclei, particle size distributions, and chemical composition. Submitted to Scientific Data 2016.
- Schrod et al., Ice nucleating particles over the Eastern Mediterranean measured from unmanned aircraft systems. In prep, to be submitted to Atmos. Chem. Phys. Disc. 2016.
- Su, H., Cheng, Y., Ma, N., Wang, Z., Wang, X., Pöhlker, M. L., Nillius, B., Wiedensohler, A., and Pöschl, U.: A broad supersaturation scanning (BS2) approach for rapid measurement of aerosol particle hygroscopicity and cloud condensation nuclei activity, Atmos. Meas. Tech., 9, 5183-5192, doi:10.5194/amt-9-5183-2016, 2016.
- Tröstl et al., (2016), Nature 533, 527-531
- Vali, G., (1971) Quantitative evaluation of Experimental Results on the Heterogeneous Freezing Nucleation of Supercooled Liquids. J. Atmos. Sci., 28, 402-409, doi: 10.1175/1520-0469
- Vergara Temprado, J., Wilson, T. W., O'Sullivan, D., Browse, J., Pringle, K. J., Ardon-Dryer, K., Bertram, A. K., Burrows, S. M., Ceburnis, D., DeMott, P. J., Mason, R. H., O'Dowd, C. D., Rinaldi, M., Murray, B. J., and Carslaw, K. S.: Contribution of feldspar and marine organic aerosols to global ice nucleating particle concentrations, Atmos. Chem. Phys. Discuss., doi:10.5194/acp-2016-822, in review, 2016.Zhu Y, et al. (2014) Satellite retrieval of convective cloud base temperature based on the NPP/VIIRS Imager. Geophys Res Lett 41(4):1308–1313.
- Yu, X., Wang, Z., Zhang, M., Kuhn, U., Xie, Z., Cheng, Y., Pöschl, U., and Su, H.: Ambient measurement of fluorescent aerosol particles with a WIBS in the Yangtze River Delta of China: potential impacts of combustion-related aerosol particles, Atmos. Chem. Phys., 16, 11337-11348, doi:10.5194/acp-16-11337-2016, 2016.